

LIGHT VECTOR MESONS IN NUCLEAR MATTERT. HATSUDA^{1,2}, H. SHIOMI² and H. KUWABARA²¹ *Institute for Nuclear Theory, University of Washington, Seattle, WA 98195, USA*² *Institute of Physics, University of Tsukuba, Tsukuba, Ibaraki 305, Japan***Abstract**

We summarize the current theoretical and experimental status of the spectral changes of vector mesons (ρ , ω , ϕ) in nuclear medium. Various approaches including QCD sum rules, effective theory of hadrons and bag models show decreasing of the vector meson masses in nuclear matter. Possibility to detect the mass shift through lepton pairs in $\gamma - A$, $p - A$ and $A - A$ reactions are also discussed.

Invited paper submitted to Prog. Theor. Phys.

1 Introduction

At high temperature (T) and density (ρ), hadronic matter is expected to undergo a phase transition to the quark-gluon plasma [1]. The order parameter characterizing the transition is the chiral quark condensate $\langle\bar{q}q\rangle$, the absolute value of which decreases as (T,ρ) increases. Numerical simulations of quantum chromodynamics (QCD) on the lattice are actively pursued to determine the precise nature of the transition at finite T [2] and various model calculations have been done to look for the observable signature of the phase transition [3].

In this article, we will concentrate on one of the interesting critical phenomena associated with the QCD phase transition, namely the spectral change of hadrons, in particular the mass shift of light vector-mesons (ρ , ω and ϕ) in nuclear matter at zero T . The vector mesons are unique in the sense that they decay into lepton pairs (e^+e^- and $\mu^+\mu^-$) which can be detected experimentally without much disturbance by complicated hadronic interactions.

In section 2, we will review the current knowledge of the quark condensate in medium. In section 3, various approaches to calculate the vector meson masses in nuclear matter are summarized. Section 4 and 5 are devoted to the detailed explanation of the mass shift of ρ , ω and ϕ in quantum hadrodynamics, an effective theory of mesons and baryons. Experimental possibilities to detect the spectral change are discussed in section 6. Concluding remarks are given in section 7.

2 Quark condensates in nuclear matter

The dynamical breaking of chiral symmetry has close similarity with the gauge-symmetry breaking in superconductors as has been first recognized by Nambu

and Jona-Lasinio [4]. Table 1 shows a brief comparison between QCD and the BCS theory for “low temperature” superconductivity.

QCD	BCS
$q - \bar{q}$ paring	$e_{\uparrow} - e_{\downarrow}$ paring
chiral symmetry breaking $\langle \bar{q}q \rangle \neq 0$	gauge symmetry breaking $\langle e_{\uparrow}e_{\downarrow} \rangle \neq 0$
quark spectrum: $E = \sqrt{p^2 + M^2}$ M (constituent quark-mass) $\simeq 350$ MeV	electron spectrum: $E = \sqrt{\epsilon(p)^2 + \Delta^2}$ Δ (BCS gap) ~ 0.01 eV
Nambu-Goldstone (NG) boson = pion	NG boson is absorbed by photon

Table 1: Comparison between the dynamical breaking of chiral symmetry in QCD and the dynamical breaking of gauge symmetry in the BCS theory.

The medium modification of the quark condensate has been calculated by various methods (lattice QCD, chiral perturbation theory, Nambu-Jona-Lasinio model etc). See a review [5] and also [6]. By these studies, it turned out that there is one noticeable difference between the behavior of $\langle \bar{q}q \rangle$ at finite T (with $\rho = 0$) and that at finite ρ (with $T = 0$): In the former case, the significant change of the condensate can be seen only near the critical point $T \sim T_c$ [7]. On the other hand, in the latter case, $O(30\%)$ change of $\langle \bar{q}q \rangle$ could be seen even in normal nuclear-matter density. This observation is based on the following formula in the fermi-gas approximation (independent particle approximation)[8]

$$\frac{\langle \bar{u}u \rangle}{\langle \bar{u}u \rangle_0} \simeq 1 - \frac{4\Sigma_{\pi N}}{f_{\pi}^2 m_{\pi}^2} \int^{p_F} \frac{d^3p}{(2\pi)^3} \frac{M_N}{E(p)} . \quad (1)$$

Here $m_N(m_\pi)$ is the nucleon (pion) mass, f_π is the pion decay constant, $\Sigma_{\pi N} = (45 \pm 10)\text{MeV}$ is the πN sigma term, and $E(p) \equiv \sqrt{p^2 + M_N^2}$. $\langle \cdot \rangle$ and $\langle \cdot \rangle_0$ denote the expectation value in nuclear matter and that in the vacuum respectively. The integration for the nucleon momentum p should be taken from 0 to the fermi momentum p_F . At normal nuclear matter density ($\rho = \rho_0 = 0.17/\text{fm}^3$), the above formula gives $(34 \pm 8)\%$ reduction of the chiral condensate from the vacuum value. In Fig.1, $\langle \bar{u}u \rangle / \langle \bar{u}u \rangle_0$ as well as the strangeness condensate $\langle \bar{s}s \rangle / \langle \bar{s}s \rangle_0$ are shown in the linear density approximation [9], where the uncertainty of $\Sigma_{\pi N}$ is considered. Estimates taking into account the fermi motion and the nuclear correlatons show that these corrections at $\rho = \rho_0$ are less than the above uncertainty [10].

Unfortunately, the condensate itself is not a direct observable and one has to look for physical quantities which are measurable and simultaneously sensitive to the change of the condensate. The masses of light vector-mesons are the leading candidates of such quantities.

Fig.1

3 Vector mesons in nuclear matter – overview

—

Let's consider ρ , ω and ϕ mesons propagating inside the nuclear matter. Adopting the same fermi-gas approximation with (1) and taking the vector meson at rest ($\mathbf{q} = 0$), one can generally write the mass-squared shift as

$$\delta m_V^2 \equiv m_V^{*2} - m_V^2 = 4 \int^{p_F} \frac{d^3p}{(2\pi)^3} \frac{M_N}{E(p)} f_{VN}(\mathbf{p}), \quad (2)$$

where $f_{VN}(\mathbf{p})$ denotes the vector-meson (V) – nucleon (N) forward scattering amplitude in the relativistic normalization, and $m_V^*(m_V)$ denotes the vector me-

son mass in nuclear matter (vacuum). Here, we took spin-isospin average for the nucleon states in f_{VN} . If one can calculate $f_{VN}(\mathbf{p})$ reasonably well in the range $0 < p < p_F = 270$ MeV (or 1709 MeV $< \sqrt{s} < 1726$ MeV in terms of the $V - N$ invariant mass), one can predict the mass shift. Unfortunately, this is a difficult task: $f_{VN}(\mathbf{p})$ is not a constant in the above range since there are at least two s-channel resonances $N(1710)$, $N(1720)$ in the above interval and two nearby resonances $N(1700)$ and $\Delta(1700)$. They all couple to the $\rho - N$ system [11] and give variation of $f_{VN}(\mathbf{p})$ as a function of p in principle. From this reason, one should develop other methods to estimate δm_V^2 without referring to the detailed form of $f_{VN}(\mathbf{p})$. We will briefly review two of such approaches in the following subsections, namely the QCD sum rules and effective theories of hadron.

3.1 QCD sum rules

This subsection is partly based on the work in ref.[12, 13]. The QCD sum rules (QSR) for vector mesons in nuclear matter were first developed by Hatsuda and Lee [12]. In their approach, one starts with the retarded current correlation function in nuclear matter,

$$\Pi_{\mu\nu}(\omega, \mathbf{q}) = i \int d^4x e^{iqx} \langle \mathbf{R} J_\mu(x) J_\nu(0) \rangle \quad , \quad (3)$$

where $q^\mu \equiv (\omega, \mathbf{q})$ and $\mathbf{R} J_\mu(x) J_\nu(0) \equiv \theta(x^0) [J_\mu(x), J_\nu(0)]$ with the source currents J_μ defined as $J_\mu^{\rho,\omega} = \frac{1}{2}(\bar{u}\gamma_\mu u \mp \bar{d}\gamma_\mu d)$ ($-(+)$ is for the $\rho^0(\omega)$ -meson) and $J_\mu^\phi = \bar{s}\gamma_\mu s$. Although there are two independent invariants in medium (transverse and longitudinal polarization), they coincide in the limit $\mathbf{q} \rightarrow 0$ and reduce to $\Pi_{\mu\mu}/(-3\omega^2) \equiv \Pi$. Π satisfies the following dispersion relation,

$$\text{Re}\Pi(\omega^2) = \frac{1}{\pi} \text{P} \int_0^\infty du^2 \frac{\text{Im}\Pi(u)}{u^2 - \omega^2} + (\text{subtraction}). \quad (4)$$

In QSR, the spectral density $\text{Im}\Pi$ is modeled with several phenomenological parameters, while $\text{Re}\Pi$ is calculated using the operator product expansion (OPE). The phenomenological parameters are then extracted by matching the left and right hand side of (4) in the asymptotic region $\omega^2 \rightarrow -\infty$. The density dependence in the OPE side is solely determined by the density dependent condensates which are evaluated from low energy theorems or from the parton distribution of the nucleon [12].

In the medium, we have three kinds of structure in the spectral density: the resonance poles, the continuum and the Landau damping contribution. For $\mathbf{q} \rightarrow 0$, the last contribution is calculable *exactly* and behaves like a pole at $\omega^2 = 0$ [12, 14]. In total, the hadronic spectral function looks as

$$\begin{aligned} 8\pi\text{Im}\Pi(u > 0^-) &= \delta(u^2)\rho_{sc} + F^*\delta(u^2 - m_V^{2*}) + (1 + \frac{\alpha_s}{\pi})\theta(u^2 - S_0^*) \quad (5) \\ &\equiv \rho_{had.}(u^2), \end{aligned}$$

with $\rho_{sc} = 2\pi^2\rho/\sqrt{p_F^2 + M_N^2} \simeq 2\pi^2\rho/M_N$. m_V^* , F^* and S_0^* are the three phenomenological parameters in nuclear matter to be determined by the sum rules.

Matching the OPE side and the phenomenological side via the dispersion relation in the asymptotic region $\omega^2 \rightarrow -\infty$, we can relate the resonance parameters to the density dependent condensates. There are two major procedures for this matching, namely the Borel sum rules (BSR) [15] and the finite energy sum rules (FESR) [16], which can be summarized as

$$\begin{aligned} \int_0^\infty ds W(s) [\rho_{had.}(s) - \rho_{OPE}(s)] &= 0, \quad (6) \\ W(s) &= \begin{cases} s^n \theta(S_0 - s) & \text{(FESR),} \\ e^{-s/M^2} & \text{(BSR).} \end{cases} \end{aligned}$$

Here the spectral function $\rho_{had.}(s)$ stands for eq.(5). $\rho_{OPE}(s)$ is a hypothetical imaginary part of Π obtained from OPE.

To make quantitative analyses of spectral parameters, the stability analysis based on the Borel transform is more suitable than FESR. Since the Borel mass M is a fictitious parameter introduced in the sum rule, the physical quantities should be insensitive to the change of M within a Borel interval $M_{\min} < M < M_{\max}$; namely the principle of minimum sensitivity (PMS) [17] is used. One can accomplish this insensitivity by choosing S_0^* suitably at given density. In Fig. 2, the Borel curves for the $\rho(\omega)$ meson for three different values of baryon density are shown with S_0^* chosen to make the Borel curve as flat as possible in the interval $0.41\text{GeV}^2 < M^2 < 1.30\text{GeV}^2$. The upper (lower) bound of the Borel interval is determined so that the power (continuum) correction after the Borel transform does not exceed 30 % of the lowest order term in OPE.

Fig.2

By making a linear fit of the result, one obtains [12, 13]

$$\frac{m_{\rho,\omega}^*}{m_{\rho,\omega}} = 1 - (0.16 \pm 0.06) \frac{\rho}{\rho_0}, \quad (7)$$

$$\sqrt{\frac{S_0^*}{S_0}} = 1 - (0.15 \pm 0.05) \frac{\rho}{\rho_0}, \quad (8)$$

$$\frac{F^*}{F} = 1 - (0.24 \pm 0.07) \frac{\rho}{\rho_0}, \quad (9)$$

and

$$\frac{m_\phi^*}{m_\phi} = 1 - (0.15 \pm 0.05) y \frac{\rho}{\rho_0}, \quad (10)$$

where y is the OZI breaking parameter in QCD defined as $y = 2\langle\bar{s}s\rangle_N/\langle\bar{u}u + \bar{d}d\rangle_N$ with $\langle\cdot\rangle_N$ being the nucleon matrix element. y takes the value 0.1 – 0.2 [12]. The decrease in eqs. (7,10) is dictated by the density dependent condensates $\langle\bar{q}q\rangle$, $\langle(\bar{q}q)^2\rangle$ and $\langle\bar{q}\gamma_\mu D_\nu q\rangle$. The errors in the above formulas are originating from the uncertainties of the density dependence of the these condensates. The contribution of the quark-gluon mixed operator with twist 4, [13] which may

possibly weaken the mass shift, is neglected in the above. Shown in Fig.3 is the mass shift given in eqs. (7,10) with possible theoretical uncertainties.

Fig.3

Some sophistications of the QSR analyses by Hatsuda and Lee have been done later by several authors.

(i) Asakawa and Ko have introduced a more realistic spectral function than (5) by taking into account the width of the ρ -meson and the effect of $\pi - N - \Delta - \rho$ dynamics [18]. By doing the similar QSR analysis as above, they found that the negative mass shift occurs also in this realistic case.

(ii) Monte Carlo based error analysis was applied to the Borel sum rule by Jin and Leinweber [19] instead of the Borel stability or PMS analysis employed in [12, 13]. They found $m_{\rho,\omega}^*/m_{\rho,\omega} = 1 - (0.22 \pm 0.08)(\rho/\rho_0)$ and $m_{\phi}^*/m_{\phi} = 1 - (0.01 \pm 0.01)(\rho/\rho_0)$, which are consistent with eqs. (7,10) within the error bars.

(iii) Koike analysed an *effective* scattering amplitude \bar{f}_{VN} defined as $\delta m_V^2 \equiv \bar{f}_{VN} \cdot \rho$ using the QSR in the vacuum [20]. Although his original calculation predicting $\bar{f}_{VN} > 0$ is in error as was pointed out in ref.[13, 19], revised calculation gives a consistent result with eqs. (7,10) within the error bars [21]. Note here that \bar{f}_{VN} does not have direct relation to the scattering length at zero momentum $f_{VN}(0)$.

3.2 Effective theories

There have been many attempts so far to calculate the spectral change of the vector mesons using effective theories of QCD. The first attempt by Chin [22] using the quantum hadrodynamics (QHD) shows increasing ω -meson mass in medium due to a process analogous to the Compton scattering;

$$\omega + N \rightarrow \omega + N. \quad (11)$$

For the ρ -meson, similar but more sophisticated calculations taking into account Δ -resonance and in-medium pion show a slight increase of the ρ -meson mass [23]. In these calculations, only the polarization of the Fermi sea (the particle-hole excitations) was considered. Also their predictions are different from the general assertion by Brown and Rho claiming that all the hadron masses except for pion should decrease [24].

On the other hand, Saito, Maruyama and Soutome [25] and Kurasawa and Suzuki [26] have realized that the mass of the ω -meson is affected substantially by the vacuum polarization of the nucleon in medium

$$\omega \rightarrow N^* \bar{N}^* \rightarrow \omega, \quad (12)$$

where N^* is the nucleon in nuclear matter which has smaller effective mass than that in the vacuum. They show that the vacuum polarization dominates over the Fermi-sea polarization in QHD and leads decreasing vector meson mass. This conclusion was later confirmed by several groups [27, 28, 29] and was generalized for the ρ and ϕ mesons by the present authors [30, 31] which will be discussed in more details in section 4 and 5. Jaminon and Ripka has also reached a similar conclusion by using a model of vector mesons coupled to constituent quarks [32].

Saito and Thomas have examined a rather different but comprehensive model (bag model combined with QHD) and found decreasing vector-meson masses [33]; $m_{\rho,\omega}^*/m_{\rho,\omega} \sim 1 - 0.09(\rho/\rho_0)$. The spectral shift of the quarks inside the bag induced by the existence of nuclear medium plays a key role in this approach.

Basic idea common in the approaches predicting the decreasing mass may be summarized as follows. In nuclear matter, scalar (σ) and vector (ω) mean-fields are induced by the nucleon sources. These mean-fields give back-reactions to the nucleon propagation in nuclear matter and modify its self-energy. This is an origin of the effective nucleon mass $M_N^* < M_N$ in the relativistic models

for nuclear matter. The same mean-fields should also affect the propagation of vector mesons in nuclear medium. In QSR, the quark condensates act on the quark propagator as density dependent mean-fields. In QHD, the coupling of the mean-field with the vector mesons are taken into account through the short distant nucleon loop with the effective mass M_N^* . In the bag-model, the mean fields outside the bag acts on quarks confined in the bag and change their energy spectrum.

Let us show here that one can understand the negative mass shift of the vector mesons in a simple and intuitive way in the context of QHD. More quantitative discussion will be given in the later section. After renormalizing infinities in the vacuum loop, the density-dependent part of the Dirac-sea polarization to the vector-meson propagator is approximately written as

$$D(q) \simeq \frac{1}{Z^{-1}q^2 - m_V^2} = \frac{Z}{q^2 - Zm_V^2}, \quad (13)$$

where Z being the finite wave-function renormalization constant in medium. The pole position is thus obtained as $m_V^* = \sqrt{Z}m_V$. Because of the current conservation, only the wave function part of the propagator is modified in medium. Since the effective mass of the nucleon decreases in medium ($M_N^*/M_N < 1$), physical vector mesons have more probability to be in virtual baryon– anti-baryon pairs compared to that in the vacuum. This means $Z < 1$, which leads to $m_V^*/m_V \equiv Z < 1$ [29, 30].

$$M_N^*/M_N < 1 \quad \rightarrow \quad Z < 1 \quad \rightarrow \quad m_V^*/m_V \equiv Z < 1 \quad . \quad (14)$$

4 ρ and ω mesons in quantum hadrodynamics

4.1 Nucleon at finite density

Before discussing the vector meson masses in medium, let's make a brief review of the effective nucleon mass at finite density in the quantum hadrodynamics (QHD) on the basis of ref.[34, 22, 35]. The lagrangian of QHD is written as

$$\begin{aligned} \mathcal{L} = & \bar{\psi}[\gamma_\mu(i\partial^\mu - g_v V^\mu) - (M_N - g_s S)]\psi \\ & + \frac{1}{2}(\partial_\mu S\partial^\mu S - m_s^2 S^2) - \frac{1}{4}F_{\mu\nu}F^{\mu\nu} + \frac{1}{2}m_v^2 V_\mu V^\mu + \mathcal{L}_{\mathcal{CT}} \quad , \end{aligned} \quad (15)$$

with

$$F_{\mu\nu} = \partial_\mu V_\nu - \partial_\nu V_\mu \quad , \quad (16)$$

where $\psi(x)$, $S(x)$ and $V(x)$ are nucleon, σ meson and ω meson field, respectively. $\sigma(\omega)$ field is coupled to nucleon current with the coupling constant $g_s(g_v)$. $\mathcal{L}_{\mathcal{CT}}$ is the counter term added to the original lagrangian in order to get the finite physical quantities.

Let's define the nucleon propagator in uniform nuclear matter,

$$iG_{\alpha\beta}(x, y) = \langle T\psi_\alpha(x)\bar{\psi}_\beta(y) \rangle \quad . \quad (17)$$

The free nucleon propagator in momentum space is expressed as

$$\begin{aligned} G^0(p) &= (\gamma \cdot p + M_N) \left\{ \frac{1}{p^2 - M_N^2 + i\epsilon} + \frac{i\pi}{E(p)} \delta(p_0 - E(p)) \theta(p_F - |\mathbf{p}|) \right\} , \\ &\equiv G_F^0(p) + G_D^0(p), \end{aligned} \quad (18)$$

where $E(p) = \sqrt{\mathbf{p}^2 + M_N^2}$ and p_F is the fermi momentum. In the relativistic Hartree approximation (RHA) [35, 22], the full nucleon propagator reads

$$G^H(p) = G^0(p) + G^0(p)\Sigma^H G^H(p), \quad (19)$$

where H denotes the Hartree approximation. A schematic diagram for $G^H(p)$ is given in Fig.4.

Fig.4

Σ^H in Fig.4 can be written as

$$\Sigma^H = \Sigma_s - \gamma_\mu \Sigma_v^\mu, \quad (20)$$

$$\Sigma_s = i \frac{g_s^2}{m_s^2} \int \frac{d^4 p}{(2\pi)^4} \text{Tr}[G^H(p)], \quad (21)$$

$$\Sigma_v^\mu = i \frac{g_v^2}{m_v^2} \int \frac{d^4 p}{(2\pi)^4} \text{Tr}[\gamma^\mu G^H(p)], \quad (22)$$

where $\Sigma_s(\Sigma_v^\mu)$ is scalar (vector) self-energy. Formal solution of eq.(19) reads

$$\begin{aligned} [G^H(p)]^{-1} &= \gamma \cdot p - M_N - \Sigma^H \\ &= \gamma \cdot (p + \Sigma_v) - (M_N + \Sigma_s), \end{aligned} \quad (23)$$

or equivalently

$$\begin{aligned} G^H(p) &= (\gamma \cdot \bar{p} + M_N^*) \left\{ \frac{1}{\bar{p}^2 - M_N^{*2} + i\epsilon} + \frac{i\pi}{E^*(p)} \delta(\bar{p}_0 - E^*(p)) \theta(p_F - |\mathbf{p}|) \right\}, \\ &\equiv G_F^H(p) + G_D^H(p), \end{aligned} \quad (24)$$

where $E^*(p) = \sqrt{\mathbf{p}^2 + M_N^{*2}}$, $\bar{p} = p + \Sigma_v$ and $M_N^* = M_N + \Sigma_s$. Eq. (24) implies that the interacting propagator can be separated into two parts: $G_F^H(p)$ which has the same form as the free nucleon propagator with the effective nucleon mass M_N^* , and $G_D^H(p)$ which depends explicitly on the fermi momentum in nuclear matter. The advantages of this separation will be discussed later.

Next we turn to discuss self-energy Σ^H in which Σ_s is related to the nucleon effective mass. For the vector self-energy, insertion of eq.(24) into eq.(22) gives,

$$\Sigma_v^\mu = 8i \frac{g_v^2}{m_v^2} \int \frac{d^4 p}{(2\pi)^4} \frac{\bar{p}^\mu}{\bar{p}^2 - M_N^{*2} + i\epsilon} - \frac{g_v^2}{m_v^2} \delta^{\mu 0} \rho_B, \quad (25)$$

where $\rho_B = \frac{\gamma}{6\pi^2} p_F^3$ is called baryon density with $\gamma = 4$ for nuclear matter. By shifting the integration variables from p to \bar{p} , the first term on the r.h.s. vanishes, namely Σ_v^μ has no divergent term. In the case of scalar self-energy, however, one

gets

$$\Sigma_s = i \frac{g_s^2}{m_s^2} \int \frac{d^4 p}{(2\pi)^4} \frac{8M_N^*}{\bar{p}^2 - M_N^{*2} + i\epsilon} - \frac{g_s^2}{m_s^2} \frac{\gamma}{(2\pi)^3} \int^{p_F} d^3 p \frac{M_N^*}{(\mathbf{p}^2 + M_N^{*2})^{1/2}}, \quad (26)$$

where the first term on the r.h.s. is divergent. To single out this divergence, we extract the infinite part using dimensional regularization:

$$\begin{aligned} \Sigma_s^{inf} &= -\frac{g_s^2}{m_s^2} \frac{\Gamma(2 - \frac{n}{2})}{2\pi^2} M_N^{*3} \\ &= -\frac{g_s^2}{m_s^2} \frac{\Gamma(2 - \frac{n}{2})}{2\pi^2} (M_N^3 + 3M_N^2 \Sigma_s + 3M_N \Sigma_s^2 + \Sigma_s^3), \end{aligned} \quad (27)$$

where Σ_s^{inf} denotes the infinite parts and the diagrammatic illustrations are depicted in Fig.5.

Fig. 5

These divergent terms are removed by defining the following \mathcal{L}_{CT} ;

$$\mathcal{L}_{CT} = \alpha_1 S + \frac{\alpha_2}{2!} S^2 + \frac{\alpha_3}{3!} S^3 + \frac{\alpha_4}{4!} S^4, \quad (28)$$

which yields new contributions, Σ_s^{CT} , to the scalar self-energy:

$$\Sigma_s^{CT} = \sum_{n=0}^3 \frac{1}{n!} \left(\frac{-g_s}{m_s^2}\right) \left(\frac{-\Sigma_s}{g_s}\right)^n \alpha_{n+1}. \quad (29)$$

The corresponding Feynman diagrams are depicted in Fig.6.

Fig. 6

$\alpha_1 - \alpha_4$ are determined so as to cancel precisely the divergent parts in (27):

$$\alpha_n = (-i)(-g_s)^n (n-1)! \int \frac{d^4 p}{(2\pi)^4} \text{Tr}[G_F^0(p)^n]. \quad (30)$$

Note that the finite parts of α_{1-4} are also fixed in the above conditions [22], which may or may not be justified and must be checked using experimental/empirical inputs. Examining this point is not a main theme of this article, and we simply take the above procedure to calculate the density dependent part

of Σ_s^H :

$$\begin{aligned}\Sigma_s^H &= -\frac{g_s^2}{m_s^2}\rho_s + \frac{g_s^2}{m_s^2}\frac{1}{\pi^2}[M_N^{*3}\log(M_N^*/M_N) \\ &\quad -M_N^2(M_N^* - M_N) - \frac{5}{2}M_N(M_N^* - M_N)^2 - \frac{11}{6}(M_N^* - M_N)^3] \\ &\equiv M_N^* - M_N,\end{aligned}\tag{31}$$

where

$$\rho_s = \frac{M_N^*}{\pi^2} \left\{ p_F E^*(p_F) - M_N^{*2} \log \left| \frac{p_F + E^*(p_F)}{M_N^*} \right| \right\}.\tag{32}$$

This expresses the effective nucleon mass including the vacuum polarization. The density dependence of the effective nucleon mass is shown in Fig.9. g_s, g_v and m_s are chosen to satisfy the saturation density for nuclear matter (-15.75 MeV) at nuclear matter density $p_F = 1.30 \text{ fm}^{-1}$: $g_s = 7.37, g_v = 10.1$ and $m_s = 458\text{MeV}$ [29]. Hence we find that effective nucleon mass has the reduction, $M_N^*/M_N = 0.730$, at nuclear matter density. As will be shown in section.4.2, the reduction plays a crucial role in studying vector meson masses at finite density.

4.2 ρ and ω mesons at finite density

This subsection is partly based on the work in ref.[30].

4.2.1 Effective lagrangian

Let's start with an interaction lagrangian of ρ, ω with the nucleon:

$$L_{int} = g_v \left[\bar{\psi} \gamma_\mu \tau^a \psi - \frac{\kappa_v}{2M_N} \bar{\psi} \sigma_{\mu\nu} \tau^a \psi \partial^\nu \right] V_a^\mu, \quad v = \{\rho, \omega\}, \tag{33}$$

where a runs from 0 through 3, V_0 (V_{1-3}) corresponds to the ω (ρ) field, τ^a is the isospin matrix with $\tau^0=1$, and M_N is the nucleon mass. The numerical values of the coupling constants (g_v, κ_v) will be given in sec. 4.2.4.

In nuclear medium, meson propagator is defined as

$$D^{\mu\nu}(x, y) = \langle TV^\mu(x)V^\nu(y) \rangle. \quad (34)$$

By using the free vector-meson propagator

$$D_0^{\mu\nu}(q) = \frac{g_{\mu\nu}}{q^2 - m^2 + i\epsilon} + \frac{1 - \lambda}{\lambda} \frac{q_\mu q_\nu}{(q^2 - m^2/\lambda + i\epsilon)(q^2 - m^2 + i\epsilon)}, \quad (35)$$

with λ being a gauge parameter in the Steukelberg formalism [41], the full propagator can be written as

$$D^{\mu\nu}(q) = D_0^{\mu\nu}(q) + D_0^{\mu\lambda}(q)\Pi_{\lambda\sigma}(q)D^{\sigma\nu}(q), \quad (36)$$

with the self-energy $\Pi_{\mu\nu}$. See Fig.7.a.

Fig.7

In the one-loop level, the density dependent part of the self-energy comes only from the nucleon-loop (Fig.7.b):

$$\Pi_{\mu\nu}^{ab}(q) = -\frac{i}{(2\pi)^4} \int d^4k \text{Tr}[\Gamma_\mu^a G^H(k+q) \tilde{\Gamma}_\nu^b G^H(k)] \quad , \quad (37)$$

where (a, b) are the isospin indices and we have used $G^H(p)$ defined in section 4.1. For the vertices, we make use of

$$\Gamma_\mu^a = g_v[\gamma_\mu \tau^a - \frac{\kappa_v}{2M_N} \sigma_{\mu\lambda} i q^\lambda \tau^a], \quad \tilde{\Gamma}_\nu^b = g_v[\gamma_\nu \tau^b + \frac{\kappa_v}{2M_N} \sigma_{\nu\lambda} i q^\lambda \tau^b] \quad . \quad (38)$$

where the relative sign of the tensor part in Γ_μ and that in $\tilde{\Gamma}_\nu$ is opposite to that in ref.[36]. The self interaction of the ρ meson gives density dependence only from two or higher loops. The coupling of ρ with in-medium pions analyzed in [23] is also the higher loop effect and will not be considered in this paper.

$\Pi_{\mu\nu}$ in (37) is composed of two parts $\Pi_{\mu\nu} = \Pi_{\mu\nu}^{0F} + \Pi_{\mu\nu}^D$: the first term corresponds to the fluctuation of the Dirac sea of the nucleons with mass M_N^* , while the second term gives the fluctuation of the Fermi sea + the Pauli blocking. The advantage of taking this separation is that Π_F^0 and Π_D satisfy current conservation

separately, i.e., $p^\mu \Pi_{\mu\nu}^{0F}(p) = p^\mu \Pi_{\mu\nu}^D = 0$ [38]. If one adopts a separation without current conservation, the corresponding self-energy induces spurious results [38]. $\Pi_{\mu\nu}^{0F}$ generally has divergences to be subtracted. We will show our subtraction procedure in section 4.2.2 and define $\Pi_{\mu\nu}^F$ as the subtracted polarization.

The vector meson propagator in the medium has a general form

$$D^{\mu\nu} = \frac{-P_L^{\mu\nu}}{q^2 - m^2 + \Pi_L} + \frac{-P_T^{\mu\nu}}{q^2 - m^2 + \Pi_T}, \quad (39)$$

where we have suppressed isospin indices (a, b) and m denotes the ρ or ω mass in the vacuum. $P_T^{\mu\nu}$ ($P_L^{\mu\nu}$) is the projection operator to the transverse (longitudinal) direction to \mathbf{q} :

$$P_T^{\mu\nu} = g^{\mu i}(g_{ij} + q_i q_j / \mathbf{q}^2)g^{\nu j}, \quad P_L^{\mu\nu} = e^\mu e^\nu \quad (40)$$

$$\text{with} \quad e^\mu = \frac{i}{\sqrt{q^2}}(|\mathbf{q}|, q_0 \mathbf{q} / |\mathbf{q}|). \quad (41)$$

$\Pi_{T,L}$ is related to $\Pi_{\mu\nu}$ as

$$\Pi_L = -(q^2 / \mathbf{q}^2) \Pi_{00}, \quad \Pi_T = (\Pi_l^l + (q_0^2 / \mathbf{q}^2) \Pi_{00}) / 2. \quad (42)$$

In this paper we will focus on $\Pi_{T,L}$ in the time like region with $\mathbf{q} = 0$ where Π_L is exactly equal to Π_T . To obtain (39), we adopt (35) with $\lambda \rightarrow \infty$ as a free propagator of the massive vector mesons.

4.2.2 Dirac sea effect and subtraction procedure

The interaction (33) is not a renormalizable one in the conventional sense. This implies that the model contains infinite series of the higher dimensional operators which play a role to cancel the divergences emerging from the loops of the lower dimensional operators [42, 43]. Instead of developing a systematic subtraction procedure, we will take a phenomenological way to extract $\Pi_{\mu\nu}^F$ from $\Pi_{\mu\nu}^{0F}$. First of all, we will normalize the propagator at zero density as $1/(q^2 - m^2)$, i.e. subtract

away both the divergent and finite parts from $\Pi_{\mu\nu}^{0F}$. This corresponds to a set of the renormalization conditions at zero density,

$$\left. \frac{\partial^n \Pi^F(q^2)}{\partial(q^2)^n} \right|_{q^2=m^2} = 0 \quad (n = 0, 1, 2, \dots, \infty). \quad (43)$$

A straightforward generalization of the above conditions to finite density reads

$$\left. \frac{\partial^n \Pi^F(q^2)}{\partial(q^2)^n} \right|_{M_N^* \rightarrow M_N, q^2=m^2} = 0 \quad (n = 0, 1, 2, \dots, \infty). \quad (44)$$

This together with a requirement that the higher dimensional counter terms are the local polynomials allow one to single out the density dependent part of $\Pi_{\mu\nu}^{0F}$ uniquely.

Our renormalization condition is different from the simple scheme $\Pi_{\mu\nu}^F = \Pi_{\mu\nu}^{0F} - \Pi_{\mu\nu}^{0F} |_{M_N^*=M_N}$. This simple scheme cannot remove the divergences such as M_N^*/ϵ and $(M_N^*)^2/\epsilon$ ($\epsilon \rightarrow 0$) induced by the ρNN tensor coupling. These divergences require the counter terms such as $S^n F_{\mu\nu} F^{\mu\nu}$ (S being the scalar field and $F_{\mu\nu}$ being the field-strength for the vector fields) which are allowed in our scheme but not in the simple scheme. Although our procedure is physically plausible, it is still “a” way to subtract the divergences among many other possibilities. For the ω meson, our procedure is equivalent to that in [28]. For m_ω^* , we have checked that the different subtraction procedures in [26, 29] does not cause more than 3% differences from ours at $\rho = \rho_0$. This is shown in Fig. 8.

Fig.8

Using the dimensional regularization and the above subtraction procedure, one obtains the following $\Pi_{\mu\nu}^F$ for the ρ and ω mesons.

$$\begin{aligned} \Pi_{\mu\nu}^{abF} &= \delta^{ab}(q_\mu q_\nu / q^2 - g_{\mu\nu})(\Pi_v^F + \Pi_{v,t}^F + \Pi_t^F) \\ \Pi_v^F &= \frac{g_v^2}{\pi^2} q^2 \int_0^1 dx x(1-x) \log \left\{ \frac{M_N^{*2} - q^2 x(1-x)}{M_N^2 - q^2 x(1-x)} \right\}, \end{aligned} \quad (45)$$

$$\Pi_{v,t}^F = \left(\frac{g_v^2 \kappa_v}{2M} \right) \frac{M_N^* q^2}{\pi^2} \int_0^1 dx \log \left\{ \frac{M_N^{*2} - q^2 x(1-x)}{M_N^2 - q^2 x(1-x)} \right\}, \quad (46)$$

$$\Pi_t^F = \left(\frac{g_v \kappa_v}{2M}\right)^2 \frac{q^2}{2\pi^2} \int_0^1 dx \{M_N^{*2} + q^2 x(1-x)\} \log \left\{ \frac{M_N^{*2} - q^2 x(1-x)}{M_N^2 - q^2 x(1-x)} \right\} \quad (47)$$

where the integrals take analytic forms:

$$\begin{aligned} & \int_0^1 dx x(1-x) \log \left\{ \frac{M_N^{*2} - q^2 x(1-x)}{M_N^2 - q^2 x(1-x)} \right\} \\ &= \frac{1}{3} \log(M_N^*/M_N) - \frac{2}{3} \left(\frac{M_N^{*2}}{q^2} - \frac{M_N^2}{q^2} \right) \\ &+ \frac{A^*}{3} \left(\frac{2M_N^{*2}}{q^2} + 1 \right) \tan^{-1}(1/A^*) - \frac{A}{3} \left(\frac{2M_N^2}{q^2} + 1 \right) \tan^{-1}(1/A), \quad (48) \end{aligned}$$

$$\begin{aligned} & \int_0^1 dx \log \left\{ \frac{M_N^{*2} - q^2 x(1-x)}{M_N^2 - q^2 x(1-x)} \right\} \\ &= 2 \log(M_N^*/M_N) + 2A^* \tan^{-1}(1/A^*) - 2A \tan^{-1}(1/A), \quad (49) \end{aligned}$$

where $A^* = \left(\left| \frac{4M_N^{*2}}{q^2} - 1 \right| \right)^{1/2}$, $A = \left(\left| \frac{4M_N^2}{q^2} - 1 \right| \right)^{1/2}$, and $4M_N^{*2} > q^2$ is assumed.

4.2.3 Fermi sea effect

Another contribution to $\Pi_{\mu\nu}$ comes from the Fermi sea and the Pauli blocking effects, which is expressed as

$$\Pi_{\mu\nu}^{abD}(q) = -\frac{i}{(2\pi)^4} \int d^4k \text{Tr}[\Gamma_\mu^a G_F(k+q) \tilde{\Gamma}_\nu^b G_D(k) + (F \leftrightarrow D)] \quad (50)$$

$$= \delta^{ab} (\Pi_v^D + \Pi_{v,t}^D + \Pi_t^D)_{\mu\nu}. \quad (51)$$

Substituting eq.(24) into eq.(50), one obtains the following form:

$$(\Pi_v^D)_{\mu\nu} = g_v^2 \bar{\Pi}_{\mu\nu}(q), \quad (52)$$

$$(\Pi_{v,t}^D)_{\mu\nu} = Q_{\mu\nu} \left(\frac{g_v^2 \kappa_v}{2M_N} \right) 4M_N^* q^2 I_0(q), \quad (53)$$

$$(\Pi_t^D)_{\mu\nu} = \left(\frac{g_v \kappa_v}{2M_N} \right)^2 q^2 \left[-\bar{\Pi}_{\mu\nu}(q) + Q_{\mu\nu} \left\{ (4M_N^{*2} + q^2) I_0(q) + \frac{\rho_s}{M_N^*} \right\} \right], \quad (54)$$

where $Q_{\mu\nu} = (q_\mu q_\nu / q^2 - g_{\mu\nu})$ and ρ_s has been defined in (32), and

$$\bar{\Pi}_{\mu\nu}(q) = \frac{2}{\pi^3} \int d^3k \frac{\theta(p_F - \mathbf{k})}{E^*(k)} \frac{1}{q^4 - 4(\mathbf{k} \cdot \mathbf{q})^2},$$

$$\times \left\{ (k \cdot q)^2 \left[g_{\mu\nu} - \frac{q_\mu q_\nu}{q^2} \right] + q^2 \left[k_\mu - \frac{k \cdot q}{q^2} q_\mu \right] \left[k_\nu - \frac{k \cdot q}{q^2} q_\nu \right] \right\}, \quad (55)$$

$$I_n(q) = J_n(q) + J_n(-q), \quad (56)$$

$$J_n(q) = \frac{-2}{(2\pi)^3} \int \frac{d^3k}{E^*(k)} \frac{\theta(p_F - \mathbf{k}) (2E^*(k) + q_0)^n}{q^2 + 2q \cdot k + i\epsilon} \Big|_{k_0=E^*(k)}. \quad (57)$$

Here we have shown only the real parts of Π_D relevant to study the pole position at $\mathbf{q} = 0$.

In the limit of $\mathbf{q} = 0$, $I_0(q)$ and $\bar{\Pi}_{T,L}(q)$ defined from $\bar{\Pi}_{\mu\nu}(q)$ read

$$\begin{aligned} \bar{\Pi}_T(q_0, \mathbf{q} = 0) &= \bar{\Pi}_L(q_0, \mathbf{q} = 0) \\ &= \frac{2}{3\pi^2} \left\{ p_F E^*(p_F) + \frac{q_0^2}{2} \log \left| \frac{E^*(p_F) + p_F}{M_N^*} \right| - \left(M_N^{*2} + \frac{q_0^2}{2} \right) A^* \tan^{-1} \left(\frac{p_F}{E^*(p_F) A^*} \right) \right\}, \\ I_0(q_0, \mathbf{q} = 0) &= \frac{1}{4\pi^2} \left\{ 2 \log \left| \frac{p_F + E^*(p_F)}{M_N^*} \right| - 2A^* \tan^{-1} \left(\frac{p_F}{E^*(p_F) A^*} \right) \right\}, \end{aligned} \quad (58)$$

where $A^* = \left(\left| \frac{4M_N^{*2}}{q_0^2} - 1 \right| \right)^{1/2}$ and $4M^{*2} > q_0^2$ is assumed.

The mixing of the ω meson and the σ meson does not contribute to the propagator as far as $\mathbf{q} = 0$ and $q_0^2 > 0$. This is because the meson self-energy relevant for the $\omega - \sigma$ mixing vanishes exactly in the time-like region with $\mathbf{q} = 0$ [39].

4.2.4 Coupling constant

Since the ωNN tensor coupling is generally small (e.g. $\kappa_\omega = 0.12$ in the vector dominance model), we take $(g_\omega, \kappa_\omega) = (10.1, 0.0)$ as a typical strength. For the ρ meson, we adopt the following two sets.

	set I	set II
g_ρ	2.63	2.72
κ_ρ	6.0	3.7

Table 2: Two sets of ρNN coupling constants. g_ρ (κ_ρ) denotes the vector (tensor) coupling.

Set I is obtained from the $N - N$ forward dispersion relation [44]. The Bonn potential of the $N - N$ force gives similar values with this set. Set II is obtained by the vector-meson dominance together with the ρ universality [45]. A major difference between the two sets is the strength of the ρNN tensor coupling. (See ref.[40] for the detailed discussion on the vector-meson coupling constants.) In our calculations, vertex form factors are not taken into account for simplicity.

4.2.5 Numerical Results

As mentioned before, we will focus on the time like region and consider the inverse propagator

$$D_T^{-1}(q_0, \mathbf{q} = 0) = q^2 - m^2 + \Pi_T^D(q_0, \mathbf{q} = 0) + \Pi_T^F(q_0^2) \quad . \quad (60)$$

Let us define two kinds of masses m_{re}^* (real mass) and m_{inv}^* (invariant mass). m_{re}^* is defined as a lowest zero of $D_T^{-1}(q_0, 0)$. It is the quantity to be compared with that in the QCD sum rules. The invariant mass m_{inv}^* is defined as a lowest zero of D_T^{-1} with Π_T^D neglected, in which case D_T^{-1} is a function of q^2 only. m_{inv}^* here contains only the fluctuation of the Dirac sea by definition.

In Fig. 9, the effective masses of ω are shown together with M_N^*/M_N . The dashed line denotes m_{inv}^*/m . One sees that Both m_{re}^* and m_{inv}^* decrease at finite density, e.g. $m_{re}^*/m \simeq 0.8$ at $\rho = \rho_0$. The behavior of $m_{re,inv}^*$ confirms the importance of the Dirac sea polarization found in previous studies [37, 26, 27, 28, 29, 30]. $m_{re}^* < m_{re}$ is caused by the fact that the physical ω is more dressed by the $N\bar{N}$ pairs in the medium since $M_N^* < M_N$ as we have discussed in sec.3.2

[29, 30].

Fig.9

In Fig. 10 and Fig. 11, we have shown the effective masses of the ρ meson with the parameter set I and set II, respectively. The strong ρNN tensor coupling plays a dominant role and gives $m_{re}^*/m \simeq 0.6 - 0.7$ at $\rho = \rho_0$. The polarization of the Dirac sea is again the most important ingredient and the suppression of the wave-function renormalization factor Z is the main reason for the mass reduction.

Fig.10 and Fig.11

It is in order here to make some remarks: The reduction of m_{re}^*/m is consistent with that in the QCD sum rules (eq.(7)) for the ω meson, and even larger reduction is observed for the ρ -meson in QHD. One should, however, notice that we neglected vertex form factors for the ρNN and ωNN couplings. Such form factors will generally attenuate the magnitude of the mass shift of ρ and ω . From Fig.9-11, one also observes considerable non-linearity of m_{re}^* as a function of density, which is contrast to the linear dependence in eq.(7).

5 ϕ meson in generalized QHD

This section is partly based on the work in ref.[31]. The ϕ -meson is a $\bar{s}s$ resonance in $J^P = 1^-$ channel with a narrow width ($m_\phi = 1019.4$ MeV and $\Gamma_\phi = 4.4$ MeV). It is a suitable probe of the partial restoration of chiral symmetry in hot/dense hadronic matter together with the ρ and ω mesons [46, 12, 47]. In this section, we start with an effective hadronic model where the ϕ -meson couples to nucleon and hyperons ($B \equiv N, \Lambda^0, \Sigma^\pm, \Sigma^0$) with the vector coupling,

$$L_{int} = \sum_B g_{\phi B} \bar{B} \gamma_\mu B \phi^\mu. \quad (61)$$

$g_{\phi B}$ is the ϕ -baryon coupling constant listed in Table 3.

Baryons	$g_{\sigma B}$	$g_{\omega B}$	$g_{\phi B}$
N	8.7	10.6	4.2*
Λ	5.2	6.9	4.9
Σ	5.2	6.9	4.9

Table 3: $g_{\sigma B}$, $g_{\omega B}$ and $g_{\phi B}$ denote σ - B scalar coupling, ω - B vector coupling, and ϕ - B vector coupling, respectively. $g_{\sigma B}$ and $g_{\omega B}$ are taken from [48].

Some remarks are in order here:

- (i) ϕ - Λ and ϕ - Σ couplings do not break the OZI rule, while the ϕ - N coupling is OZI violating.
- (ii) Ξ is neglected, since its effect to the ϕ self-energy is doubly suppressed by the mass of Ξ and by the OZI violation in ϕ - Ξ coupling.
- (iii) If one relies on the quark counting rule [49], the ϕ -hyperon couplings are related to the ω -hyperon couplings as $g_{\phi\Lambda(\phi\Sigma)} = g_{\omega\Lambda(\omega\Sigma)}/\sqrt{2}$ with $g_{\omega\Lambda(\omega\Sigma)}$ being determined by the fit of the hypernuclear levels [48]. This is assumed in Table 3.
- (iv) OZI violating ϕ -nucleon coupling is not known experimentally. A study of the electromagnetic form-factors of the nucleon, however, yields an upper bound of its strength [50]: $g_{\phi N}/g_{\omega N} < 0.4$.

For the non-strange nuclear matter, effects of the hyperons to the ϕ -meson self-energy arise only through hyperon-anti-hyperon loops, while the nucleon contribution to the self energy has both $N - \bar{N}$ loop and the Compton-type process. The one-loop self energy from hyperon and nucleon contributions reads

$$\Pi_{\mu\nu}^B(q) = -\frac{i}{(2\pi)^4} \int d^4k g_{\phi B}^2 \text{Tr}[\gamma_\mu G^H(k+q)\gamma_\nu G^H(k)] \quad , \quad (62)$$

where $G^H(k)$ denotes baryon propagator in nuclear matter given in (24) with M_N^* replaced by M_B^* .

Although one can calculate the density dependence of M_B^* within QHD as in sec.3.1, we take here the following simple ansatz to illustrate the essential feature of the correlation between M_B^* and m_ϕ^* :

$$g_{\sigma\Lambda(\sigma\Sigma)}/g_{\sigma N} = (M_{\Lambda(\Sigma)} - M_{\Lambda(\Sigma)}^*)/(M_N - M_N^*), \quad (63)$$

$$M_N^*/M_N \simeq 1 - 0.15(\rho/\rho_0). \quad (64)$$

Eq.(63) is an universal relation in QHD [48] and Eq.(64) is a simple parametrization of the effective nucleon mass which sometimes used in the literatures for $\rho < 2\rho_0$ (see, e.g. [28]). In Fig. 12, effective masses of N , Λ and Σ parametrized by eqs. (63,64) are shown as a function of baryon density.

Fig.12

The ϕ -meson mass m_ϕ^* in medium is obtained as a solution of the dispersion relation

$$\omega^2 - m_\phi^2 + \sum_B \Pi_B(\omega, \mathbf{0}) = 0, \quad (65)$$

where $\Pi_B(\omega, \mathbf{0}) \equiv -\Pi_B^{\mu\mu}(\omega, \mathbf{0})/3\omega^2$, and m_ϕ is the ϕ -meson mass in the vacuum. $\Pi_B^{\mu\mu}$ is assumed to be a renormalized self-energy with the same subtraction procedure in the previous section.

In Fig.13, the ratio m_ϕ^*/m_ϕ calculated with only the hyperon-loops is shown by the solid line. m_ϕ^* decreases by 6% at $\rho = \rho_0$. Note that the Okubo-Zweig-Iizuka (OZI) rule is preserved for ϕ -hyperon vertices, while it is violated in the self-energy Π_B . This is because the self-energy represents interaction of ϕ ($s\bar{s}$ pair) with *non-strange* nuclear matter. Similar phenomena are known in two-step decay processes such as $\phi \rightarrow K\bar{K} \rightarrow \rho\pi$, $f' \rightarrow K\bar{K} \rightarrow \pi\pi$, and $J/\psi \rightarrow D\bar{D} \rightarrow \rho\pi$,

where each vertex preserves the OZI rule while the whole amplitude does violate the rule [51].

Fig.13, and Fig.14

The solid line in Fig.14 shows the ratio m_ϕ^*/m_ϕ calculated with only the nucleon-loops. Since $g_{\phi N}$ is not known experimentally, the result in this case has much uncertainty compared to the hyperon case. We have used $g_{\phi N}/g_{\omega N} = 0.32$ in Fig.14 which is close to the upper bound given in Table 3: thus the resultant decrease of m_ϕ^* in Fig.14 should be considered as an upper limit. The negative mass shift in Fig.13 and Fig.14 is a direct consequence of the current conservation ($\partial_\mu(\bar{B}\gamma^\mu B) = 0$) and $M_B^*/M_B < 1$ as discussed in sec.3.2. This mechanism is quite general and does not depend on the details of the interaction and on the virtual particles running in the loop.

To see the effect of the ultraviolet cutoff on the finite part of the loop integral in (62), let us define $\Pi_B^{\mu\mu}(\omega, \mathbf{0}; \Lambda_{cut}) \equiv \Pi_B^{\mu\mu}(\omega, \mathbf{0}; \Lambda_{cut}) - \Pi_B^{\mu\mu}(\omega, \mathbf{0}; \Lambda_{cut})|_{\rho=0}$ and use this in (65). We take covariant cutoff for Λ_{cut} for simplicity. When $\Lambda_{cut} \rightarrow \infty$, $\Pi_B(\omega, \mathbf{0}; \Lambda_{cut})$ reduces to the renormalized $\Pi_B(\omega, \mathbf{0})$. The dashed lines in Fig.13 and Fig.14 are the results of such calculations for three cases, $\Lambda_{cut} = 1, 2, 10$ GeV. Although the cutoff dependence is not negligible, the qualitative picture we draw in the above is not affected.

We have considered only the nucleon and hyperon loops in the ϕ self-energy. Another possible contribution is the kaon-loop in medium. This was studied by Ko et al. [47] who found that the kaon-loop has a tendency to decrease m_ϕ^* at low densities provided that the effective kaon mass $\bar{m}_K^* = (m_{K^-}^* + m_{K^+}^*)/2$ decreases in medium. However, whether \bar{m}_K^* really decreases in nuclear matter or not is still a controversial issue (see e.g. [52]).

6 Experiments

How one can detect the spectral change of vector mesons in experiments? One of the promising ideas is to use heavy nuclei and produce vector mesons in $\gamma - A$ or $p - A$ reactions. Suppose one could create a vector meson at the center of a heavy nucleus. (It does not matter whether it is created at the nuclear surface or at the center as far as the produced vector mesons run through the nucleus before the hadronic decay). It is easy to see that the number of lepton pairs decaying inside the nucleus $N_{in}(l^+l^-)$ and that outside the nucleus $N_{out}(l^+l^-)$ are related as

$$\frac{N_{in}(l^+l^-)}{N_{out}(l^+l^-)} \sim \frac{1 - e^{-\Gamma_{tot}R}}{e^{-\Gamma_{tot}R}} \quad , \quad (66)$$

where Γ_{tot} denotes the total width of vector mesons ($(1.3\text{fm})^{-1}$, $(23\text{fm})^{-1}$ and $(45\text{fm})^{-1}$ for ρ , ω and ϕ , respectively) and R being the nuclear radius. Eq.(66) shows that even the ϕ meson has considerable fraction of N_{in}/N_{out} if the target nucleus is big enough.

There exist already some proposals to look for the mass shift of vector mesons in nuclear medium [53]. One is by Shimizu et al. who propose an experiment to create ρ and ω in heavy nuclei using coherent photon - nucleus reaction and subsequently detect the lepton pairs from ρ and ω . Enyo et al. propose to create ϕ meson in heavy nuclei using the proton-nucleus reaction and to measure kaon pairs as well as the lepton pairs. By doing this, one can study not only the mass shift but also the change of the leptonic vs hadronic branching ratio $r = \Gamma(\phi \rightarrow e^+e^-)/\Gamma(\phi \rightarrow K^+K^-)$. Since m_ϕ is very close to $2m_K$ in the vacuum, any modification of the ϕ -mass or the K -mass changes the ratio r substantially as a function of mass number of the target nucleus. Similar kinds of experiments are also planned at CEBAF and GSI.

There are also on-going heavy ion experiments at SPS (CERN) and AGS (BNL) where high density matter is likely to be formed. In particular, CERES/NA45 and HELIOS-3 at CERN reported enhancement of the lepton pairs below the ρ resonance [54, 55], which may not be explained by the conventional sources of lepton pairs. E859 at BNL-AGS reported a possible spectral change of the ϕ -peak in K^+K^- spectrum [56]. If these effects are real, low mass enhancement of the lepton pair spectrum expected by the mass shift of the vector mesons could be a possible explanation [57] (see also [58] for another explanation). In nuclear collisions at higher energies (RHIC and LHC), hot hadronic matter or possibly the quark-gluon-plasma with low baryon density are expected to be formed. In such cases, double ϕ -peak structure proposed by Asakawa and Ko [47] as well as the spectral change of ρ and ω [59] will be a distinct signal of the chiral restoration in QCD.

7 Concluding remarks

The spectral change of the elementary excitations in medium is an exciting new possibility in QCD. By studying such phenomenon, one can learn the structure of the hadrons and the QCD ground state at finite (T, ρ) simultaneously. Theoretical approaches such as the QCD sum rules and the hadronic effective theories predict that the light vector mesons (ρ , ω and ϕ) are sensitive to the partial restoration of chiral symmetry in hot/dense medium. These mesons are good probes experimentally, since they decay into lepton pairs which penetrate the hadronic medium without losing much information. Thus, the lepton pair spectroscopy in QCD will tell us a lot about the detailed structure of the hot/dense matter, which is quite similar to the soft-mode spectroscopy by the photon and

neutron scattering experiments in solid state physics.

This work was supported by the Grants-in-Aids of the Japanese Ministry of Education, Science and Culture (No. 06102004). T. H. thanks Institute for Nuclear Theory at the University of Washington for its hospitality and the Department of Energy for partial support during the completion of this work.

Figure Captions

Fig.1 The light quark condensates in N=Z nuclear matter in the linear density approximation. Theoretical uncertainty of the πN sigma term is taken into account. We take $y = 0.12$ for the OZI breaking parameter, where $y \equiv 2\langle\bar{s}s\rangle_N/\langle\bar{u}u + \bar{d}d\rangle_N$ with $\langle\cdot\rangle_N$ being the nucleon matrix element.

Fig.2 Borel curve for the $\rho(\omega)$ meson mass. Solid, dashed and dash-dotted lines correspond to $\rho/\rho_0 = 0, 1.0$ and 2.0 respectively. $S_0^*(\rho)$ determined by the Borel stability method at each density is also shown in GeV^2 unit. The Borel window is chosen to be $0.41\text{GeV}^2 < M^2 < 1.30\text{GeV}^2$.

Fig.3 Masses of ρ, ω and ϕ mesons in nuclear matter predicted in the QCD sum rules. The hatched region shows theoretical uncertainty.

Fig.4 Feynman diagram of the relativistic Hartree approximation (RHA). The wavy (dashed) line is the vector (scalar) meson propagator. The double (single) solid line denotes the Hartree (free) propagator of the nucleon.

Fig.5 An illustration of the divergent parts of Σ_s . The dashed line is the scalar meson propagator and the double (single) solid line denotes the Hartree (free) propagator of the nucleon.

Fig.6 An illustration of the contribution from counter terms. Crosses denote the insertion of the counter terms with coefficients $\alpha_1 - \alpha_4$.

Fig.7 (a) The Dyson equation for the vector meson propagator with self-energy Π . The double (single) wavy line is the full (free) vector-meson propagator. (b) Vector-meson self-energy in the one-loop approximation. The double solid line denotes the nucleon propagator in the Hartree approximation.

Fig.8 Effective ω meson mass as a function of the baryon density using three different subtraction procedures for meson self-energy. The solid, dashed

and dash-dotted lines are obtained by the subtraction schemes given in ref.[29],[30] and [26], respectively. Triangle, diamond and square denote the values at $\rho = \rho_0$ in each subtraction scheme.

Fig.9 Effective masses of the nucleon and the ω meson as a function of the baryon density. m_{re}^* (m) denotes the real mass in the medium (the mass in vacuum). The dashed line corresponds to the invariant mass in the medium.

Fig.10 Real and invariant masses of the ρ -meson in the parameter set I, $(g_\rho, \kappa_\rho)=(2.63,6.0)$.

The dashed line corresponds to m_{inv}^*/m .

Fig.11 Same quantities with Fig.10 in the parameter set II, $(g_\rho, \kappa_\rho)=(2.72,3.7)$.

The dashed line corresponds to m_{inv}^*/m .

Fig.12 Ratio of the baryon mass in matter M_B^* and that in vacuum M_B ($B = N, \Lambda, \Sigma$) as a function of ρ/ρ_0 . This figure is taken from ref.[31].

Fig.13 Ratio of the ϕ -meson mass in matter m_ϕ^* and that in the vacuum m_ϕ as a function of ρ/ρ_0 . Only hyperon contributions are included in the ϕ -meson self-energy. This figure is taken from ref.[31].

Fig.14 Same with Fig.13 except that only the nucleon contribution is included.

This figure is taken from ref.[31].

References

- [1] See e.g. Proceedings of Quark Matter '95, Nucl. Phys. **A590** (1995) Nos. 1,2.
- [2] A. Ukawa, *Lectures on Lattice QCD at Finite Temperature*, UTHEP-302 (1995).
- [3] T. Hatsuda, *Hadron Structure and the QCD Phase Transition*, hep-ph/9502345 (1995); R. Pisarski, *Applications of Chiral Symmetry*, hep-ph/9503330 (1995); G. E. Brown and M. Rho, *Chiral Restoration in Hot and/or Dense Matter*, hep-ph/9504250 (1995).
- [4] Y. Nambu and G. Jona-Lasinio, Phys. Rev. **122** (1961) 345.
- [5] T. Hatsuda and T. Kunihiro, Phys. Rep. **247** (1994) 221.
- [6] T. Hatsuda and T. Kunihiro, Phys. Rev. Lett. **55** (1985) 158, Prog. Theor. Phys. **74** (1985) 765, Phys. Lett. **B185** (1987) 304.
- [7] P. Gerber and H. Leutwyler, Nucl. Phys. **B321** (1989) 387.
- [8] E. G. Drukarev and E. M. Levin, Prog. Part. Nucl. Phys. **A556** (1991) 467; T. Hatsuda, H. Hogaasen and M. Prakash, Phys. Rev. Lett. **66** (1991) 2851; T. D. Cohen, R. J. Furnstahl and D. K. Griegel, Phys. Rev. Lett. **67** (1991) 961.
- [9] T. Hatsuda, Nucl. Phys. **A544** (1992) 27c.
- [10] T. D. Cohen, R. J. Furnstahl and D. K. Griegel, Phys. Rev. **C45** (1992) 1881. G. Q. Li and C. M. Ko, Phys. Lett. **B338** (1994) 118.
- [11] Review of Particle Properties, Phys. Rev. **D50** (1994) No.3.
- [12] T. Hatsuda and S. H. Lee, Phys. Rev. **C46** (1992) R34.
- [13] T. Hatsuda, S. H. Lee and H. Shiomi, Phys. Rev. **C52** (1995) 3364 .
- [14] A. L. Bochkarev and M. E. Shaposhnikov, Nucl. Phys. **B268** (1986) 220.

- [15] A. Shifman, A. I. Vainshtein and V. I. Zakharov, Nucl. Phys. **B147** (1979) 385.
- [16] N. V. Krasnikov, A. A. Pivovarov and N. N. Tavkhelidze, Z. Phys. **C19** (1983) 301.
- [17] P. M. Stevenson, Phys. Rev. **D23** (1981) 2916.
- [18] M. Asakawa and C. M. Ko, Phys. Rev. **C48** (1993) 526.
- [19] X. Jin and D. B. Leinweber, Phys. Rev. **C52** (1995) 3344.
- [20] Y. Koike, Phys. Rev. **C51** (1995) 1488.
- [21] Y. Koike, private communication.
- [22] S. A. Chin, Ann. Phys. **108** (1977) 301.
- [23] M. Asakawa, C. M. Ko, P. Levai and X. J. Qiu, Phys. Rev. **C46** (1992) R1159. M. Herrmann, B. L. Friman and W. Noerenberg, Nucl. Phys. **A560** (1993) 411.
- [24] G. E. Brown and M. Rho, Phys. Rev. Lett. **66** (1991) 2720.
- [25] K. Saito, T. Maruyama and K. Soutome, Phys. Rev. **C40** (1989) 407.
- [26] H. Kurasawa and T. Suzuki, Prog. Theor. Phys. **84** (1990) 1030.
- [27] K. Tanaka, W. Bentz and A. Arima and F. Beck, Nucl. Phys. **A528** (1991) 676.
- [28] J. C. Caillon and J. Labarsouque, Phys. Lett. **B311** (1993) 19.
- [29] H.-C. Jean, J. Piekarewicz and A. G. Williams, Phys. Rev. **C49** (1994) 1981.
- [30] H. Shiomi and T. Hatsuda, Phys. Lett. **B334** (1994) 281.
- [31] H. Kuwabara and T. Hatsuda, Prog. Theor. Phys. **96** (1995) 1163.
- [32] M. Jaminon and G. Ripka, Nucl. Phys. **A564** (1993) 505.

- [33] K. Saito and A. W. Thomas, Phys. Rev. **C51** (1995) 2757, *ibid.* **C52** (1995) 2789.
- [34] J. D. Walecka, Ann. Phys. (N. Y.) **83** (1974) 491.
- [35] B. D. Serot, J. D. Walecka, *Advances in Nuclear Physics*, edited by J. W. Negele and E. Vogt (Plenum, New York, 1986), Vol.16.
- [36] L. S. Celenza, A. Pantziris and C. M. Shakin, Phys. Rev. **C 45** (1992) 205.
- [37] R. J. Furnstahl and C. J. Horowitz, Nucl. Phys. **A485** (1988) 632.
- [38] J. F. Dawson, R. J. Furnstahl, Phys. Rev. **C 42** (1990) 2009.
- [39] K. Lim, C. J. Horowitz, Nucl. Phys. **A501** (1989) 729.
- [40] R. Machleidt, in *Advances in Nuclear Physics*, edited by J. W. Negele and E. Vogt (Plenum, New York, 1989), Vol. 19.
- [41] C. Itzykson and J-B. Zuber, *Quantum Field Theory*, section 12-5-2, (McGraw-Hill, New York, 1980).
- [42] S. Weinberg, Physica **96A** (1979) 327.
- [43] J. Polchinski, Lectures at *TASI '92*, UTTG-20-92 (1992).
- [44] W. Grein, Nucl. Phys. **B131** (1977) 255; W. Grein and P. Kroll, Nucl. Phys. **A338** (1980) 332.
- [45] J. J. Sakurai, *Currents and Mesons*, (Univ. of Chicago Press, Chicago, 1969).
- [46] D. Lissauer and E. V. Shuryak, Phys. Lett. **B253** (1991) 15;
P. Bi and J. Rafelski, Phys. Lett. **B262** (1991) 485;
J. P. Blaizot and R. Mendez Galain, Phys. Lett. **B271** (1991) 32.
- [47] C. M. Ko, P. Levai, X. J. Qiu and C. T. Li, Phys. Rev. **C45** (1992) 1400.
K. L. Haglin and C. Gale, Nucl. Phys. **B421** (1994) 613.

- M. Asakawa and C. M. Ko, Phys. Rev. **C50** (1994) 3064; Nucl. Phys. **A572** (1994) 732.
- [48] N. K. Glendenning et al., Phys. Rev. **C48** (1993) 889.
- [49] See e.g., J. J. J. Kokkedee, *The Quark Model*, (Benjamin, 1969, New York).
- [50] R. L. Jaffe, Phys. Lett. **B229** (1989) 275.
- [51] H. Lipkin, Int. J. of Mod. Phys. **E1** (1992) 603.
- [52] H. Yabu, F. Myhrer and K. Kubodera, Phys. Rev. **D50** (1994) 3549; V. P. Pandharipande, C. J. Pethick and V. Thorsson, Phys. Rev. Lett. **75** (1995) 4567.
- [53] H. Shimizu, private communication.
H. Enyo, in *Properties and Interactions of Hyperons*, ed. B. Gibson, P. Barnes and K. Nakai (World Scientific, 1994, Singapore); KEK-PS proposal (1994).
- [54] G. Agakichev et al., Phys. Rev. Lett. **75** (1995) 1272; CERES Collaboration, J. P. Wurm, Nucl. Phys. **A590** (1995) 103c.
- [55] HELIOS-3 Collaboration, M. Masera, Nucl. Phys. **A590** (1995) 93c.
- [56] B. Cole, Nucl. Phys. **A590** (1995) 179c.
- [57] G. Q. Li, C. M. Ko and G. E. Brown, Phys. Rev. Lett. **75** (1995) 4007.
- [58] G. Chanfray, R. Rapp and J. Wambach, Phys. Rev. Lett. **76** (1996) 368.
- [59] R. Furnstahl, T. Hatsuda, S. H. Lee, Phys. Rev. **D42** (1990) 1744; T. Hatsuda, Y. Koike and S.H. Lee, Nucl. Phys. **B394** (1993) 221.

Fig.1

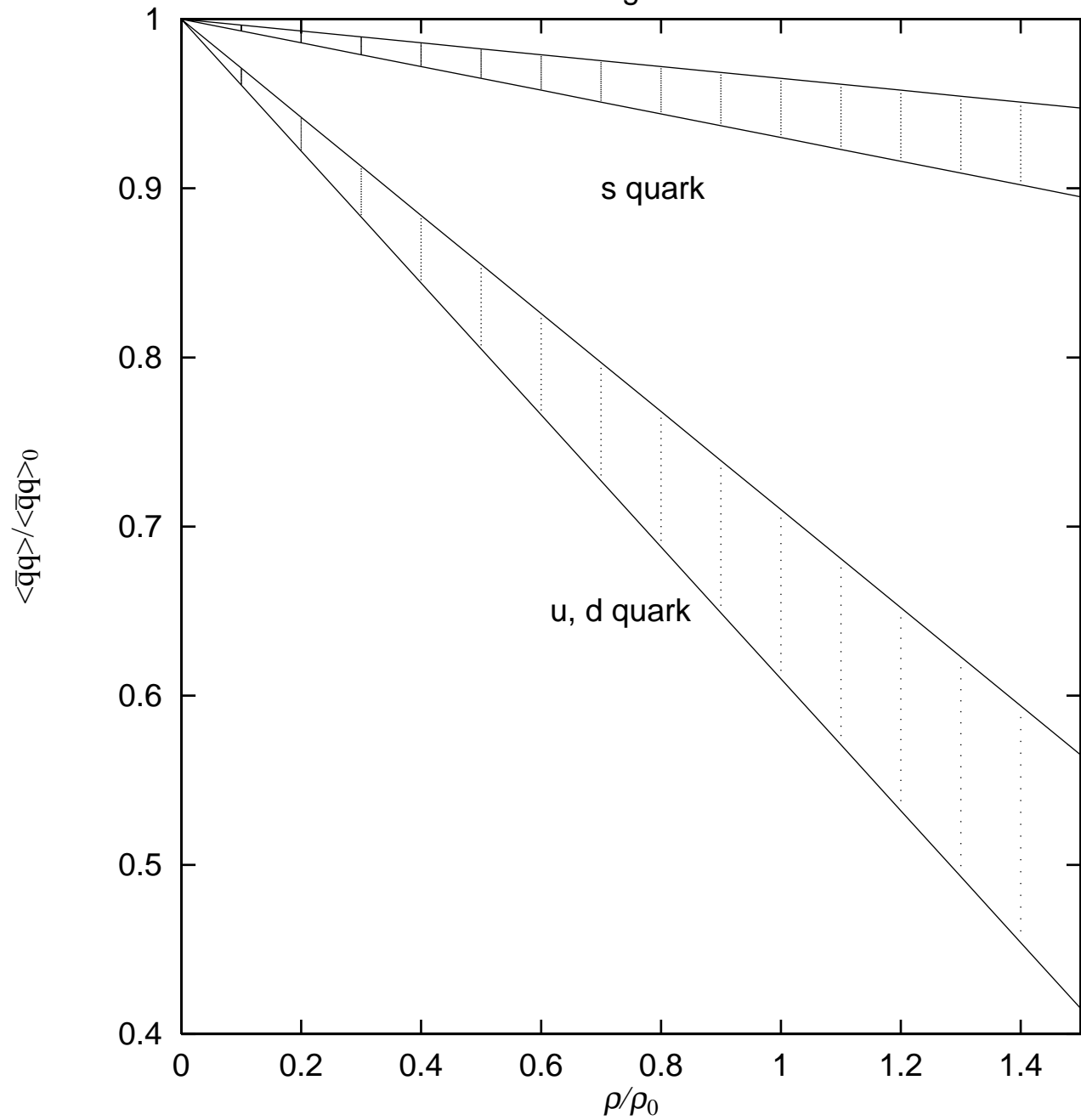


Fig.2

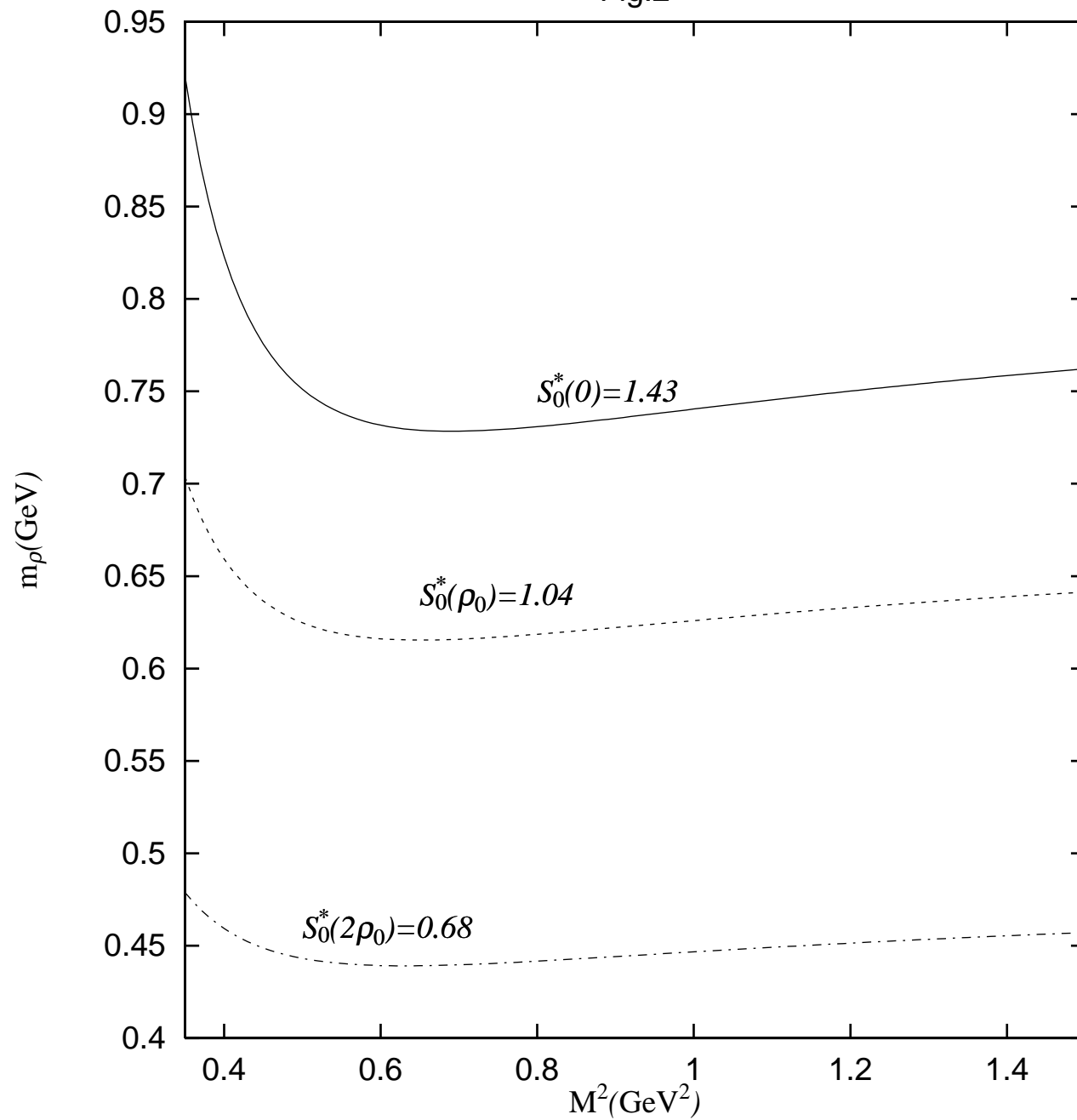


Fig.3

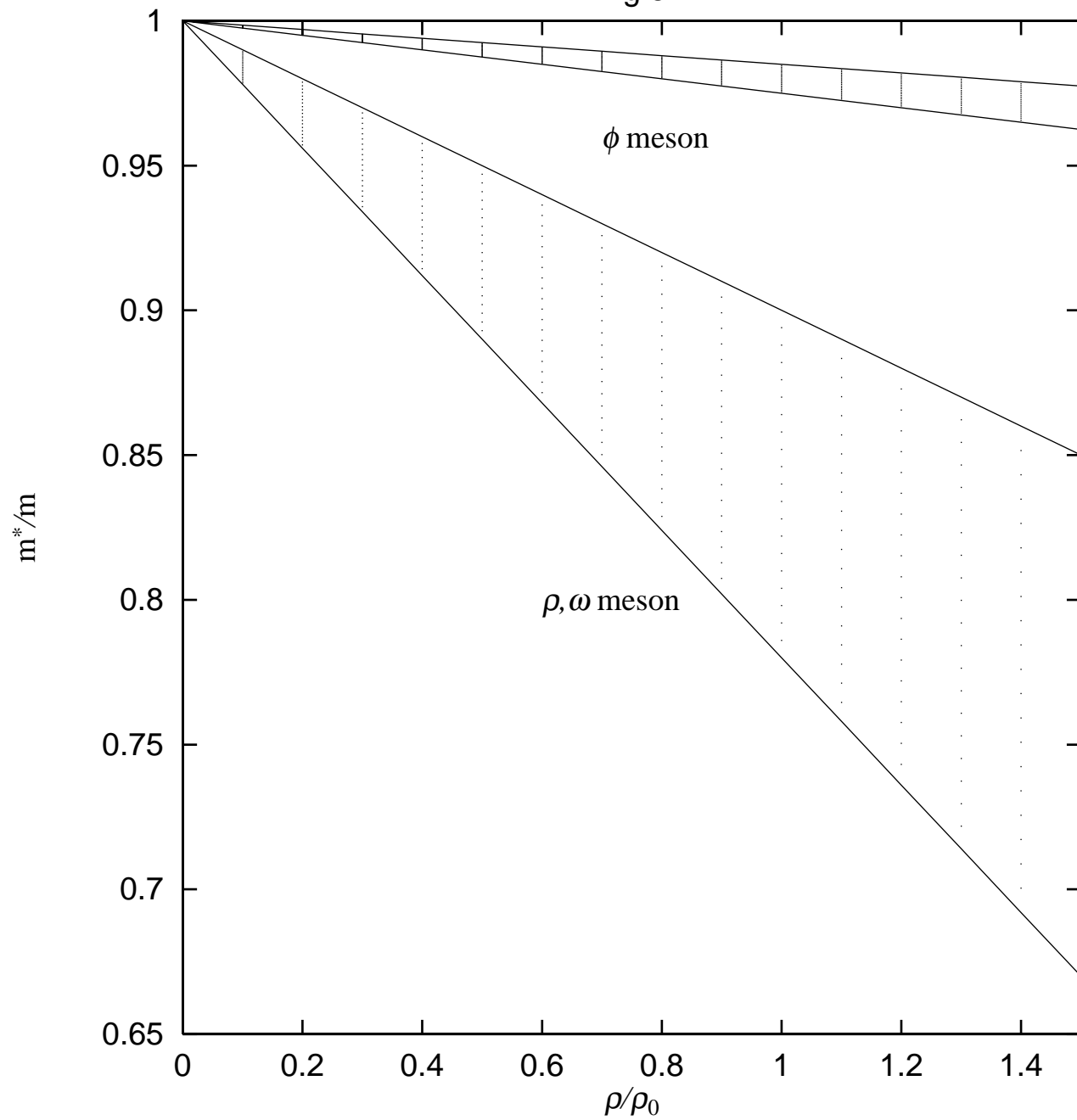


Fig.8

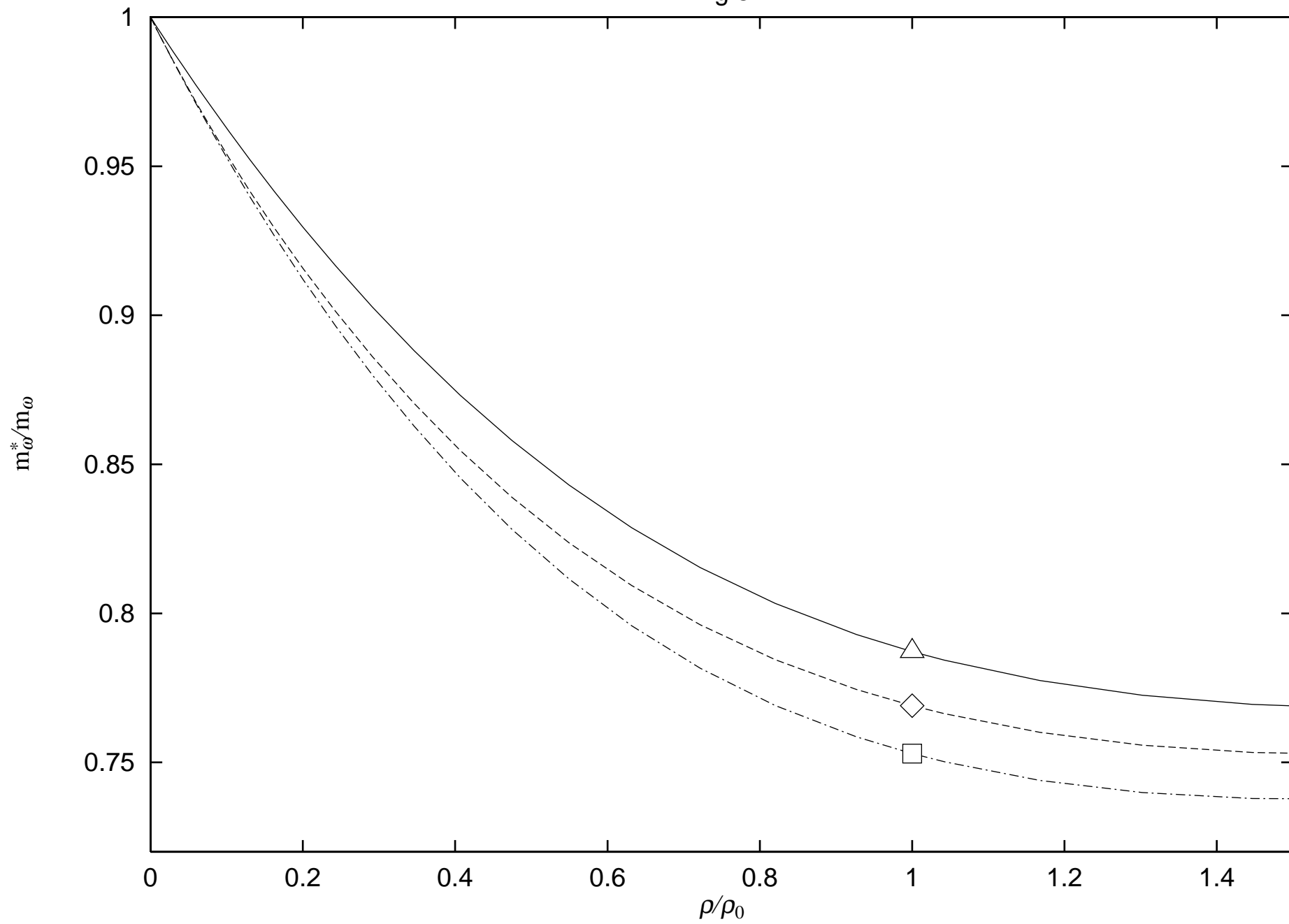


Fig.9

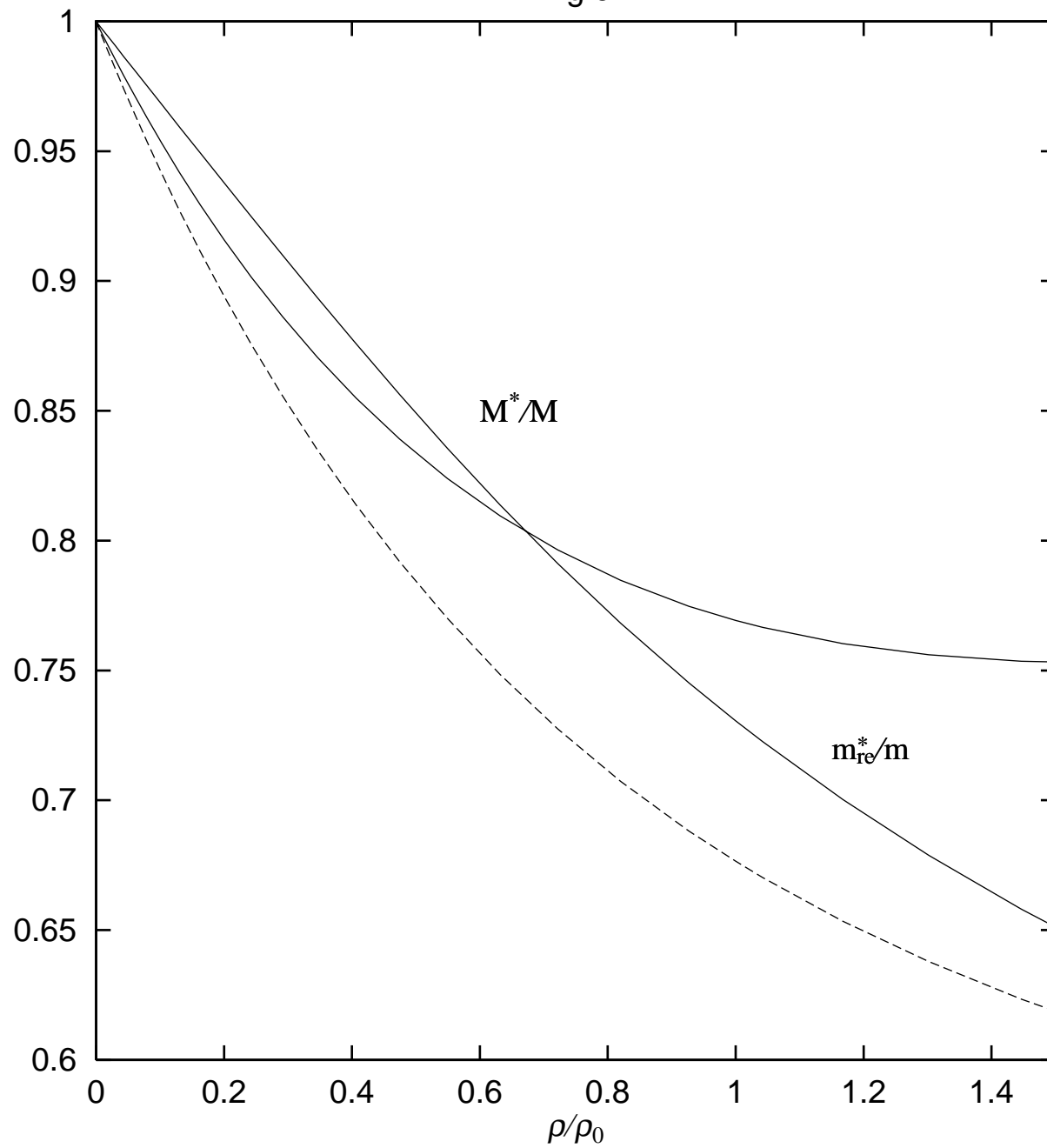


Fig.10

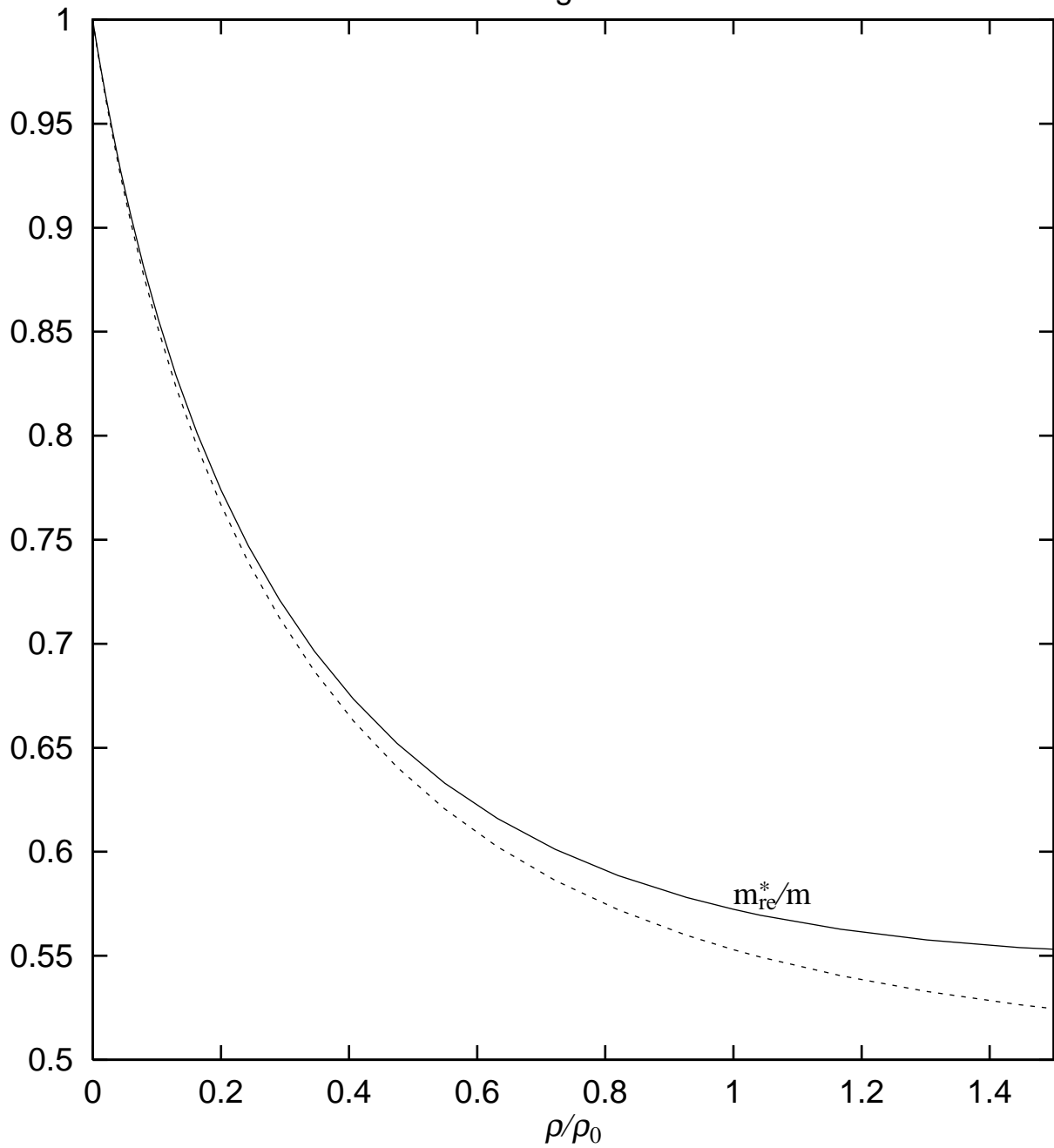
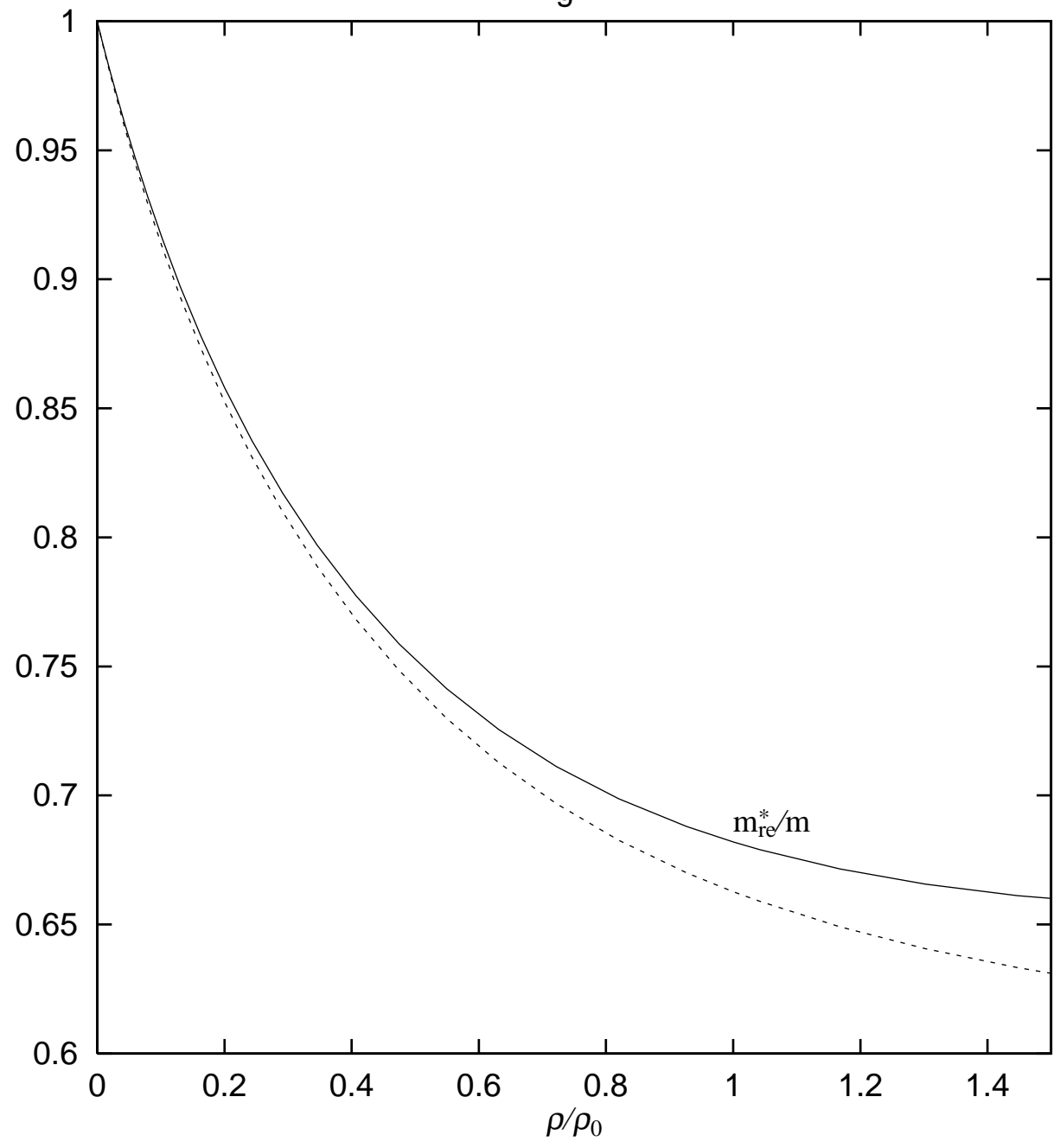


Fig.11



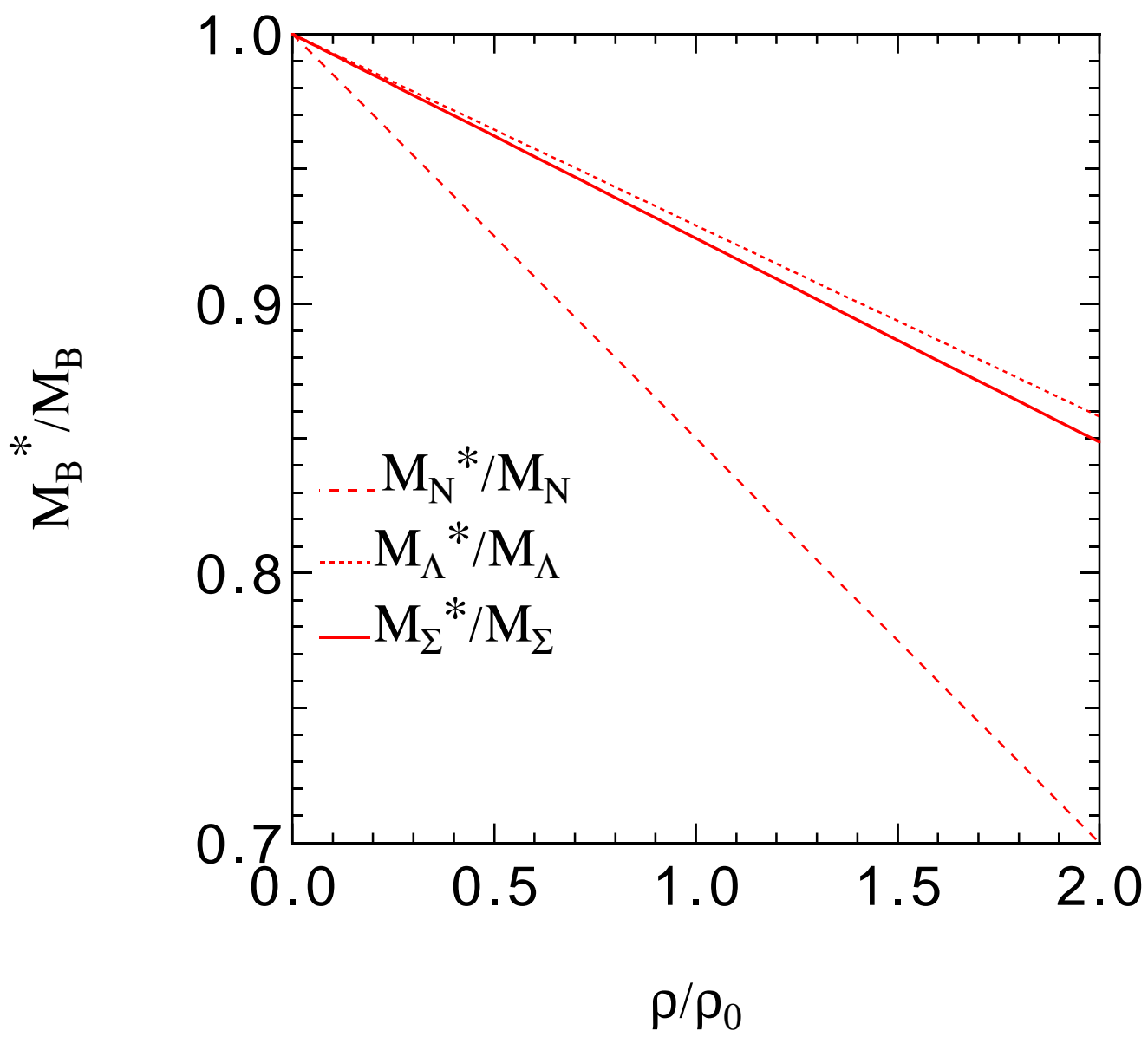


Fig.12

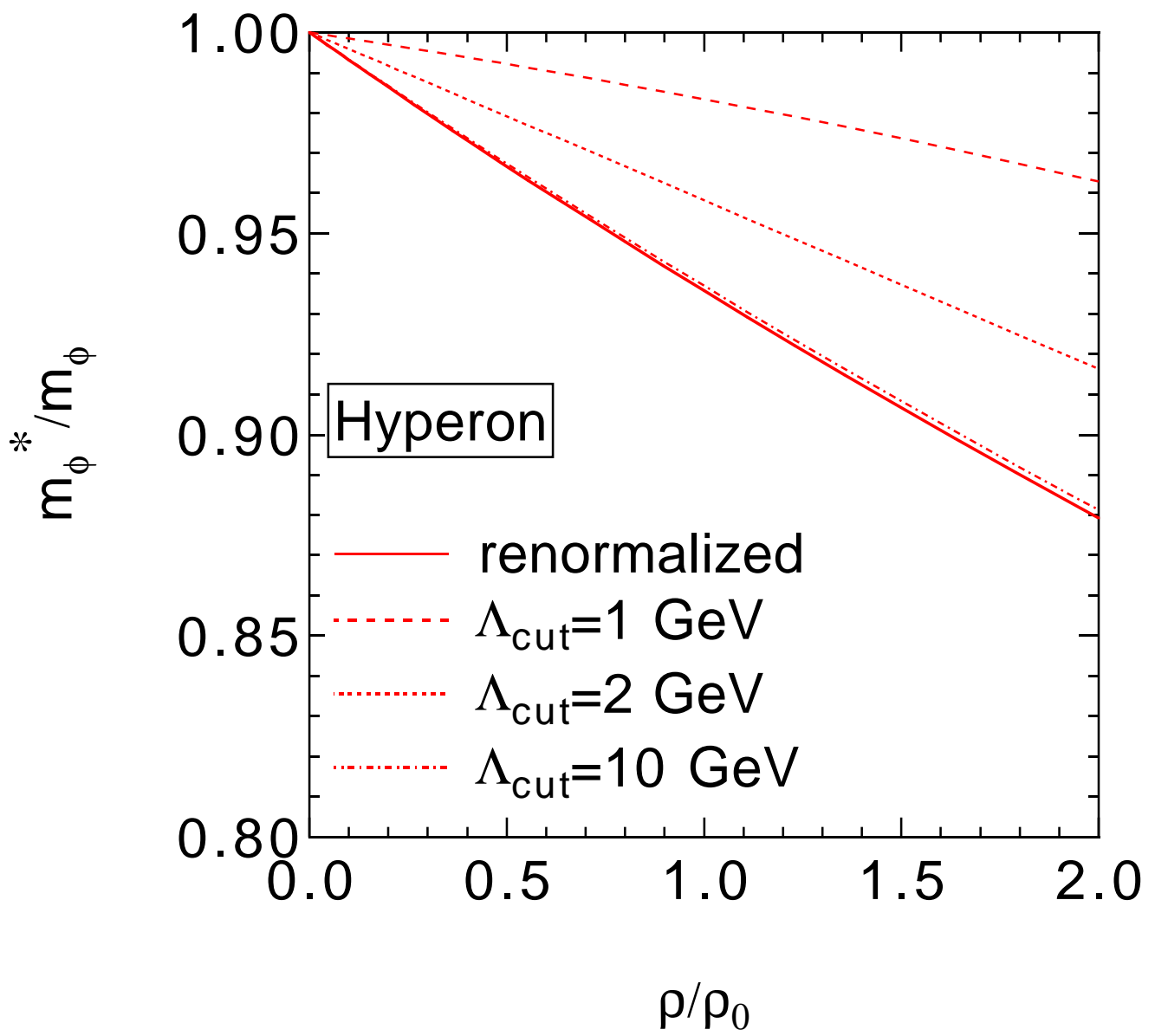


Fig.13

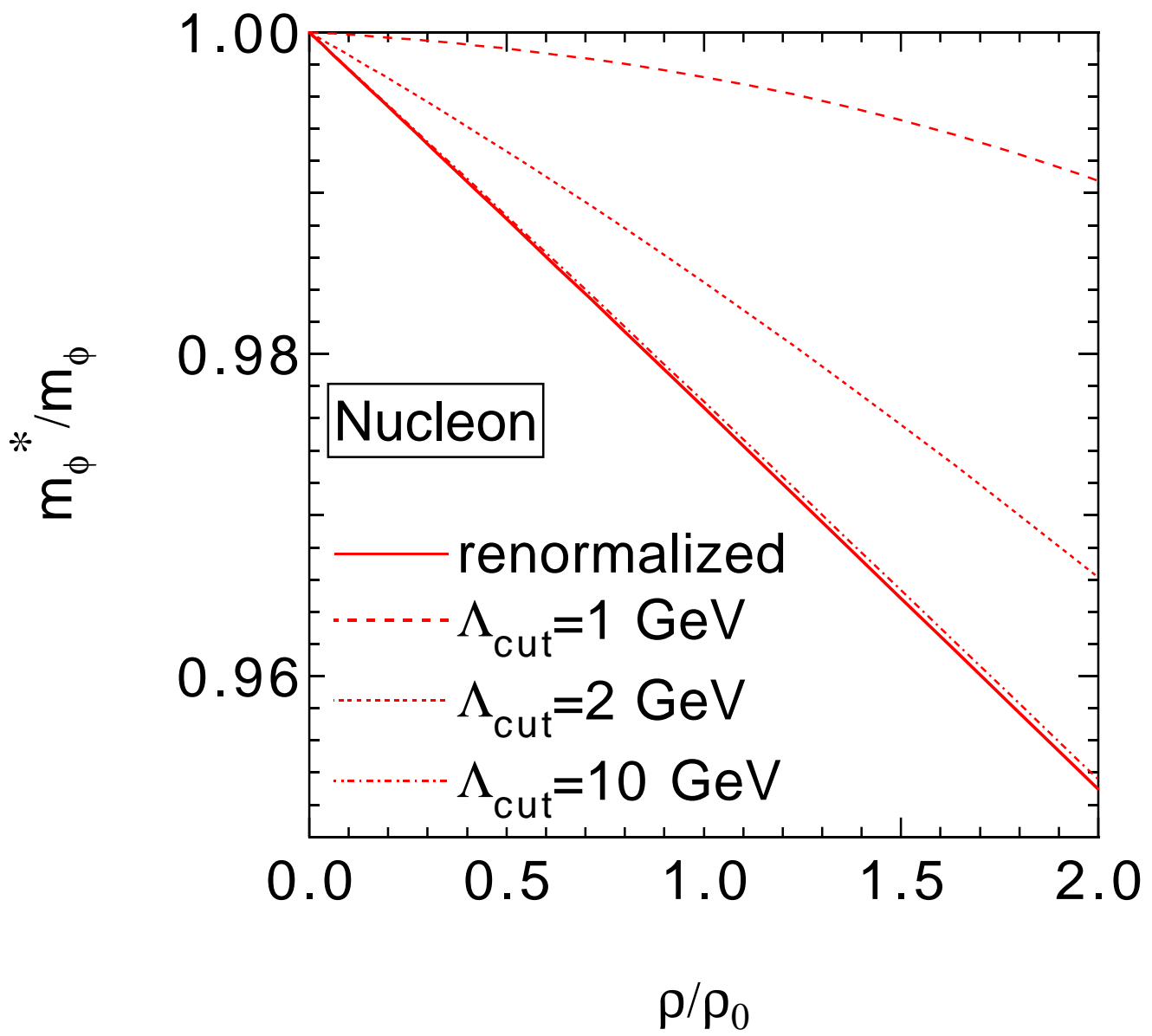


Fig.14

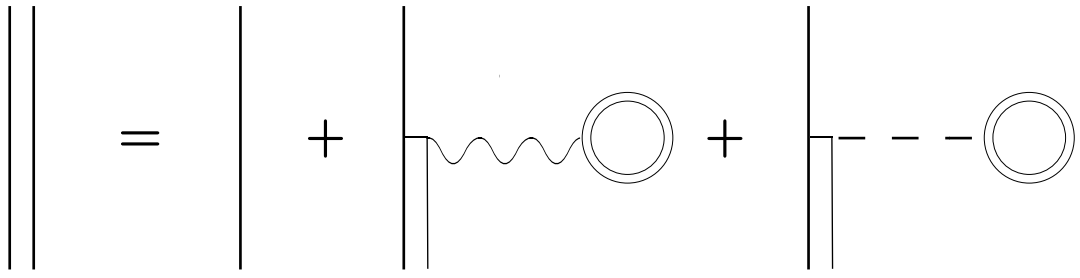


Fig. 4

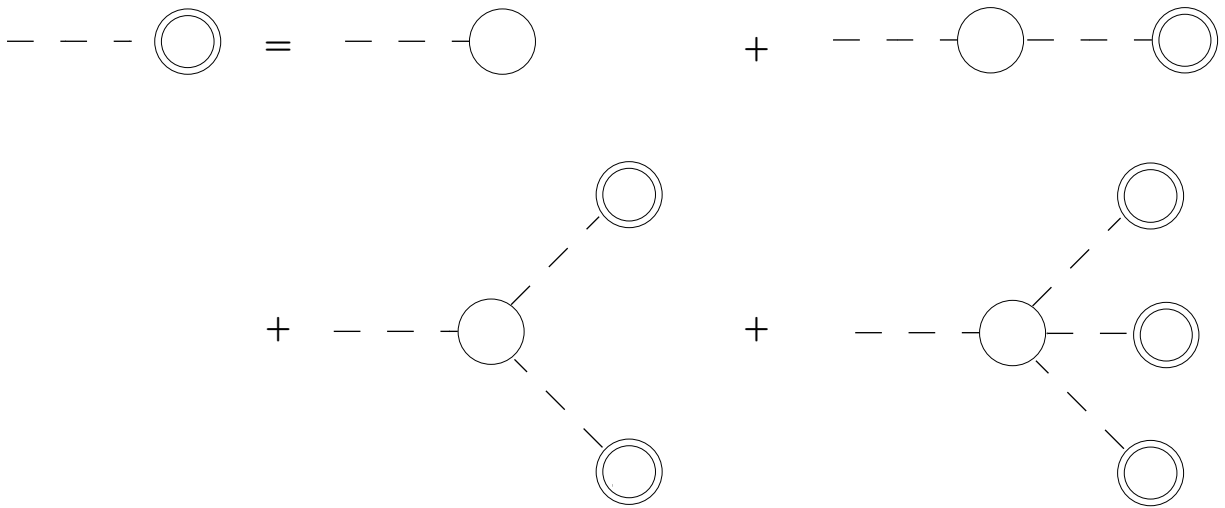


Fig. 5

$$\Sigma_s^{inf} = \text{---} \times \alpha_1 + \text{---} \times \alpha_2 \text{---} \text{---} \text{---} \text{---} \text{---}$$

Fig. 6

$$\text{---} = \text{---} + \text{---} \text{---} \text{---} \text{---} \text{---}$$

Fig . 7 (a)

$$\text{---} = \text{---}$$

Fig . 7 (b)